ACS OMEGA

http://pubs.acs.org/journal/acsodf

Article

Theoretical Investigation of Regiodivergent Addition of Anilines and Phenolates to *p*-Benzoquinone Ring

Haroldo C. Da Silva,* Talita O. C. Leite, Searitha C. Rodrigues, Beatriz L. C. De Carvalho, Maria Tereza Martins, Rodolfo G. Fiorot, Flaviana R. F. Dias, Vinícius R. Campos, Vitor F. Ferreira, Anna C. Cunha,* and Wagner B. De Almeida*

Cite This: *ACS Omega* 2022, 7, 40241−40256

Read Online

ACCESS | Metrics & More | Article Recommendations | Supporting Information

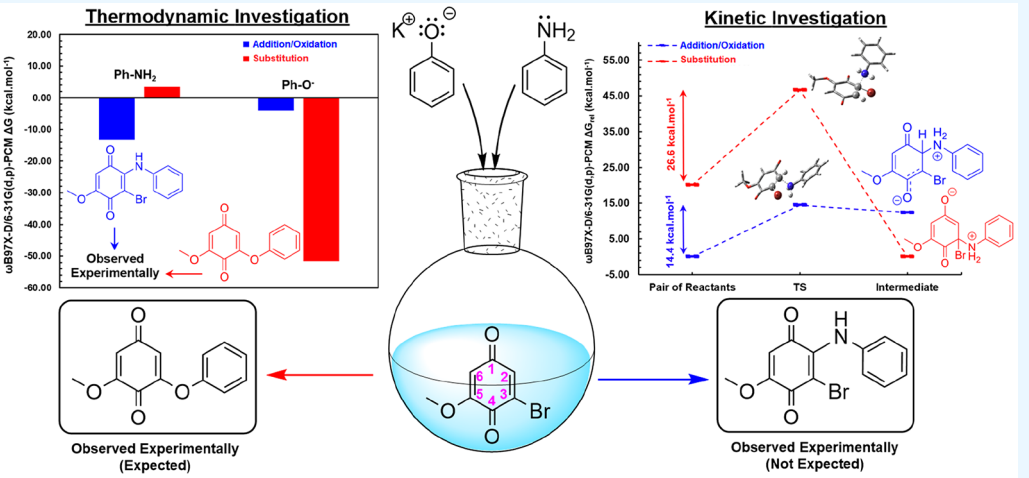

ABSTRACT: Two different products were obtained by the regiodivergent reaction of benzoquinone derivatives with phenolates and anilines: 3-aryloxybenzoquinone and 2-phenylamino-3-bromobenzoquinone. Calculated density functional theory free energies of reaction values corroborate the experimental observation of the formation of the substitution product in the reaction with phenolates in acetonitrile and the product of addition/oxidation for the reaction with aniline in water. Calculated charges and Fukui functions are similar for C2 and C3 atoms, indicating an equal possibility to suffer a nucleophilic attack. The calculated energy barriers for nucleophilic attack steps indicated that the first steps of the substitution with phenolates and addition/oxidation with anilines are faster, which justifies the formation of the respective products. The natural bond order analysis for the transition states revealed that there is a strong interaction between lone pairs of N and O atoms and the π^*_{C2C3} for the O → C2 and N → C3 attacks and a weak interaction for the O → C3 and N → C2 attacks, which also agrees with experimental observations.

1. INTRODUCTION

Quinone compounds are widely distributed in different families of plants, fungi, and some animals; many of them play integral roles in vital biochemical processes, such as coenzyme Q10 (CoQ10, **1**) or ubiquinone, an essential quinone for cellular respiration and adenosine triphosphate (ATP) production.[1] Though the benzoquinone ring constitutes a common structural unit of well-known antitumoral drugs[2] (as will be exemplified by the compounds **1**−**5** in Figure 1) such as mitomycin (**2**), mitoxantrone (**3**), and doxorubicin (**4**), this class of compounds also displays other significant pharmacological activities, such as antimicrobial and fungicide.[3,4] Benzoquinones and related compounds can exert their therapeutic effect by acting as prooxidants, reducing oxygen to reactive oxygen species (ROS), and as electrophiles, forming covalent bonds with tissue nucleophiles.[5] Most of its redox effects are based on electrophilic reactivity determined by carbonyl groups and the reaction of polarized C═C bonds with O-, N-, and S-nucleophiles.[6] Another important quinone, alizarin (**5**), serves as pigments for textiles and to improve the efficiency of dye-sensitized solar cells.[7]

Due to the versatile biological activity and chemical reactivity of quinones, our research group has explored

Received: August 12, 2022
Accepted: October 14, 2022
Published: October 26, 2022

© 2022 The Authors. Published by American Chemical Society

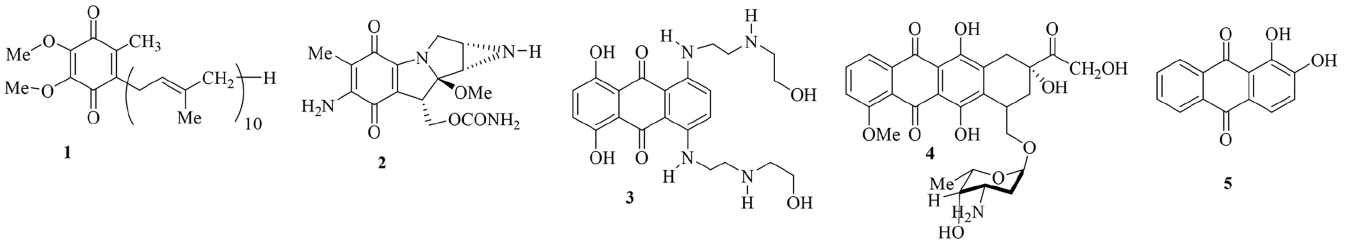

Figure 1. Different applications for quinone compounds **1**, **2**, **3**, **4**, and **5**.

Scheme 1. Synthesis Examples Involving Haloquinone Derivatives

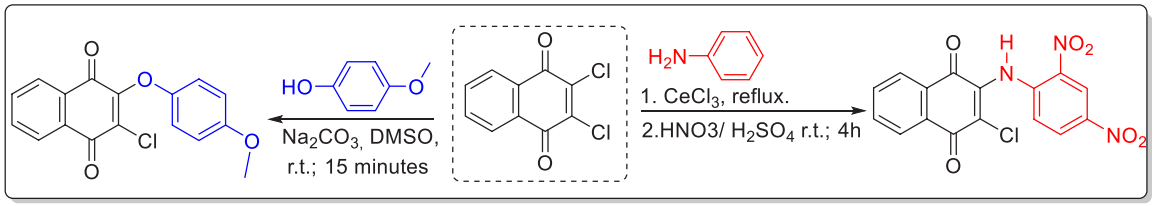

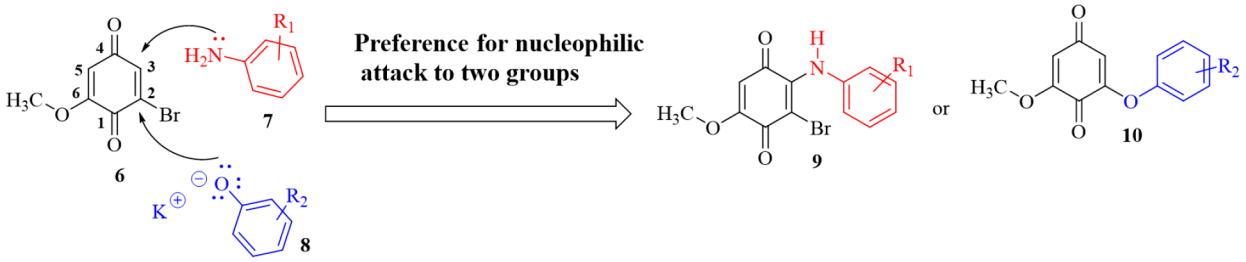

Figure 2. Regiodivergence of the nucleophilic attack.

Scheme 2. Global Equations for the (A, B) Substitution and (C, D) Addition/Oxidation Reactions with Aniline and Phenolates

A. Generic global equation for the substitution reaction with phenolates

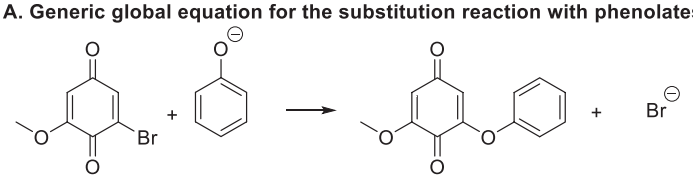

B. Generic global equation for the substitution reaction with anilines

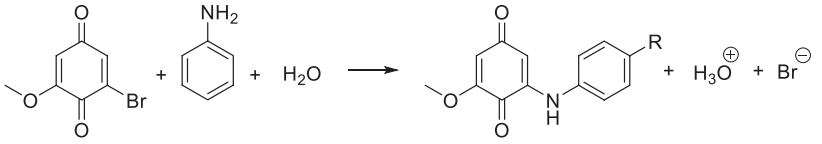

C. Generic global equation for the addition/oxidation reaction with anilines

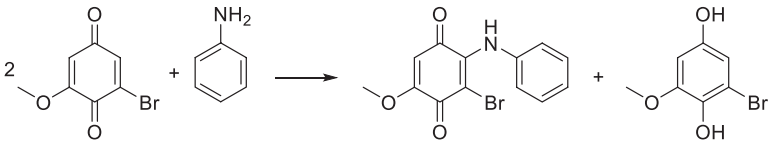

D. Generic global equation for the addition/oxidation reaction with phenolates

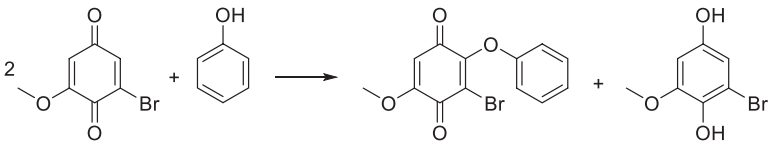

different methodologies that lead to the development of synthetically modified compounds.[5,8−10] Within this context, we report the synthesis of aminobenzoquinones **9** and aryloxybenzoquinone derivatives **10** via regiodivergent conjugate nucleophilic addition of amines **7** and phenoxides **8** to the 2-bromo-1,4-benzoquinone ring of compound **6**, which is a

https://doi.org/10.1021/acsomega.2c04607
ACS Omega 2022, 7, 40241−40256

potential synthetic building block in the design of biological molecules. It was expected that the reaction with anilines would produce the elimination of the Br atom by a substitution mechanism, but, surprisingly, the halogen atom remained in the product, generating an addition/oxidation product. In contrast to Michael addition, the nucleophilic substitution of a bromide atom by sodium phenoxides preferentially produced the quinone derivatives **10**. In short, aromatic amines were more likely to attack compound **6** by Michael addition instead of nucleophilic substitution. Other examples involving nucleophilic addition to the halo-quinone ring have been reported in the literature (Scheme 1).[11−13]

This paper aims at the theoretical investigation of this regiodivergence and the unexpected nucleophilic attack on carbon C2, using a quantum-chemical method of calculation.

2. METHODOLOGY

We started by performing a conformational analysis of the reactant **6** (2-bromine-6-methoxy-1,4-benzoquinone) through a relaxed scan calculation for the C1−C6−O−CH_3 torsion angle in the gas phase (see Figure 2). To do so, we chose the Density Functional Theory (DFT) ωB97X-D[14] functional with the Pople basis set 6-31G(d,p)[15] to represent the electrons in C, H, O, and N atoms and the core pseudopotential LANL2DZ[16] for the electrons in the bromine atoms as a computational method. This DFT functional provides reliable values for energies due the inclusion of dispersion terms,[14] which are relevant to our evaluations since the molecules investigated here have high polarizabilities. This previous analysis is important because structure **6** will be strongly discussed in terms of its molecular properties and will be part of the product molecules. The lowest-energy conformer will be considered for all calculations, using the same functional and basis set, but including the implicit solvent effects of water (dielectric constant ε = 78.36) and acetonitrile (dielectric constant ε = 35.67) by the polarizable continuum model (PCM)[17] approach.

To assess possible thermochemical preferences for the four distinct processes (nucleophilic conjugate addition/oxidation at C3 and nucleophilic substitution at C2), we computed the variation of Gibbs free energies (ΔG_r) for each global equation shown in Scheme 2, obtained by the sum of the steps described in the Supporting Information (Figures S1−S4). For the substitution mechanism with phenolate (Figure S1), the nucleophile attacks the brominated carbon, and the electrons move to the C4═O direction. The intermediate formed eliminates the halide (weaker base than the phenolate anion), regenerating the quinone moiety in the second step. For the reaction with aniline (Figure S2), on the other hand, the nucleophilic attack gives a zwitterionic intermediate, which is deprotonated in the second step by a water molecule. The last step is equivalent to that in Figure S1. The expected yield for this reaction is lower than that for the reaction with phenolates, due to the less basic character of the Ph−NH_2 (when compared to Ph−O^-) and the competition between the aniline/substrate and aniline/water interactions.

Reactions of amines with *p*-benzoquinones have been investigated before but with different proposals. Hewgill and Mullings presented a reactional route involving the nucleophilic attack on atom C3, followed by an oxidation step caused by the oxygen from the air.[18] In a very similar way, Tandon and Maurya studied substitution and addition reactions of 1,4-substituted quinones with aromatic amines in aqueous medium (reactional conditions very similar to those presented in this work) and proposed an addition/oxidation mechanism but changed the oxidizing agent (from O_2 to the quinone itself, which seems more coherent, due to the low concentration of O_2 in aqueous solution).[19] The organic product presents the initial bromine atom. The addition/oxidation mechanisms for the reaction with aniline and phenolate are presented in Figures S3 and S4, respectively.

To investigate kinetic aspects that might be involved in the regiodivergent formation of the products, we computed the energy barriers ($\Delta G_r^{\ddagger}$) of the first steps for each mechanism presented in Figures S1−S4 (no intrinsic reaction coordinate (IRC) calculations were done). These are the steps of the new forming bonds (C−N/C−O). We calculated energy barrier values as the difference between the transition-state energies and their respective prereactant complex, all fully optimized with the same computational method for the conformational analysis. The nature of these stationary points was characterized by frequency calculations, in which the minimum energy points presented exclusively positive values and the transition states exhibited only one imaginary frequency.

Natural bond order (NBO) analysis is known for describing phenomena involving electron density transfer, such as intermolecular forces[20,21] and interactions between the highest occupied molecular orbital (HOMO) and the lowest unoccupied molecular orbital (LUMO),[22,23] which are related to stabilization energy ($E(2)$), estimated by the second-order perturbative approach

$$E(2) = q_i \frac{[F(i,j)]^2}{\varepsilon_j - \varepsilon_i}$$

in which q_i is the occupancy of the bond orbital, ε_j and ε_i are the energies of the natural orbitals (acceptor and donor, respectively), and $F(i,j)$ is the Fock operator.[24−28] An NBO analysis was done for the frontier orbital interactions in the transition states (TSs), using NBO 3.1 software[29] (included in Gaussian 09 software[30]). Atomic partial charges were calculated using different models: Mulliken (MPA),[31] charges from electrostatic potentials using a grid-based method (CHELPG),[32] Hirshfeld (HPA),[33−35] its improvement, proposed by Marenich et al. (called CM5),[36] and natural charges (NPA)[37] at the ωB97X-D/6-31G(d,p)-LANL2DZ-PCM level (water and acetonitrile solvents).

An NBO analysis of the intermolecular interactions established by the nucleophile and substrate was performed in combination with the noncovalent interaction (NCI) method, which allows us to calculate the reduced density gradient (RDG), expressed mathematically by the function $s(r)$, obtained from the electron density ($\rho(r)$), using[38]

$$s(r) = \frac{|\nabla\rho(r)|}{2(3\pi^2)^{1/3}\rho(r)^{4/3}}$$

The NCI representation in two dimensions (2D) and three dimensions (3D) were obtained from Multiwfn software,[39] and, for the 2D NCI scatter map (RDG × sign(λ_2)ρ(a.u)), negative values of sign(λ_2)ρ(a.u) indicate attractive interactions (where $\rho(r)$ is the electron density and λ_2 is the second eigenvalue of the Hessian matrix).

Mulliken populational analysis is well-known for providing unphysical partial charges and being dramatically dependent on the basis set.[40] The CM5 model has been pointed out to be accurate in charge calculations for organic[41] and inorganic[42]

https://doi.org/10.1021/acsomega.2c04607
ACS Omega 2022, 7, 40241−40256

Scheme 3. Synthesis of Amino-Benzoquinone Derivatives 9a−9g and 6-Aryloxy Compounds 10a−10d

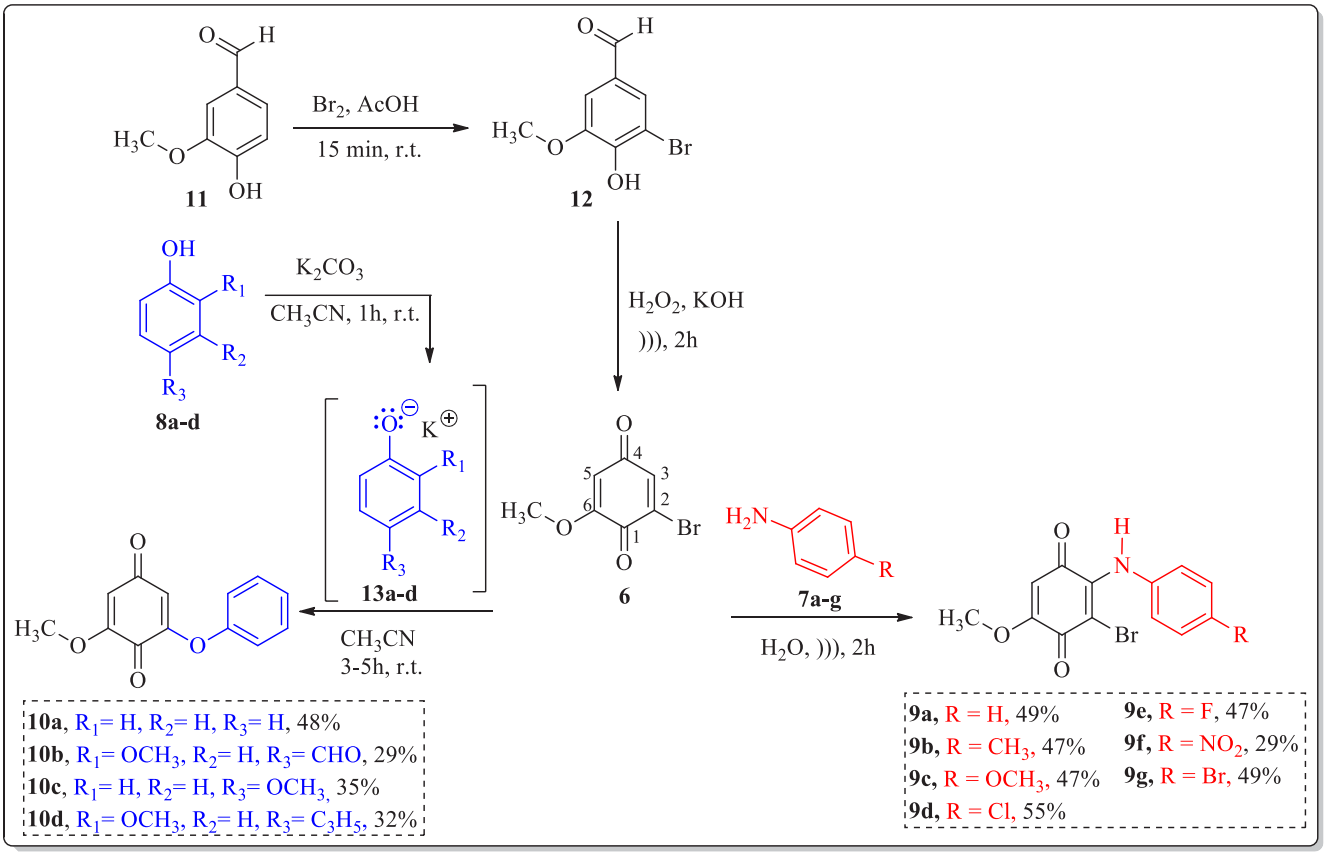

compounds. In a very recent study of regiodivergence in organic reactions involving isoquinolinequinones, Kenouche et al. carried out a benchmarking aiming to use an adequate model to describe the partial charges in the reactants. Comparing the results, they have shown an increase in performance (an indication of the robustness of the method) in the following order: Mulliken < Hirshfeld < CHELPG < NPA methods.[43] All these charge models were used in the calculations for the *p*-bromobenzoquinone molecule investigated here, with emphasis placed on the NPA charges.

The Fukui functions and hardness and softness concepts are useful tools in describing the reactivity of organic molecules[44,45] and have been largely employed in theoretical works[46−48] to provide insights about the interactions between the reactants or even to describe biological interactions.[49,50] In general, hard nucleophiles tend to react with hard electrophiles, in which their reactive sites tend to be highly charged and relatively unpolarizable. Similarly, soft nucleophiles have a high tendency to react preferentially with soft electrophiles due to their high polarizability and low charge concentration. The hardness and softness can be calculated using the ionization energy, which can be approximated as the negative of the HOMO energy, according to the frozen orbital approximation (Koopman's theorem)[51] and the electron affinity (approximately the negative of the LUMO energy by the Koopman theorem), as is shown in the following two equations, where η and S represent the global hardness and softness, respectively.[52]

$$\eta = \frac{\mathrm{IE} + \mathrm{EA}}{2}$$

$$S = \frac{1}{\mathrm{IE} + \mathrm{EA}}$$

As chemical reactions involve the redistribution of the electron density, this variation can be described by a Fukui function, defined by[53]

$$f(r) = \frac{\partial \rho(r)}{\partial N}$$

For molecules, the derivative mentioned above is not continuous and, therefore, is difficult to evaluate. Thus, alternative proposals have been developed to calculate Fukui functions numerically and approximately for a specific atom *i*. The most common is expressed by

$$f_i^+ = [\rho_i(N+1) - \rho_i(N)]$$

$$f_i^- = [\rho_i(N) - \rho_i(N-1)]$$

$$f_i^0 = \frac{[\rho_i(N+1) - \rho_i(N-1)]}{2}$$

The $\rho_i(N+1)$, $\rho_i(N)$, and $\rho_i(N-1)$ values are the electron densities associated with the atom *i* in the molecular cation, the neutral molecule, and the molecular anion, respectively. Different methods have been applied to calculate Fukui functions.[54,55] Mineva has dedicated efforts in developed methods to describe the reactivity,[56,57] and, recently, Mineva et al. proposed two alternative ways to obtain Fukui indices, based on Kohn−Sham orbitals and the atomic resolved hardness matrix.[58,59] Yang and Mortier proposed a condensed and approximated way to calculate the local Fukui functions, in

https://doi.org/10.1021/acsomega.2c04607
ACS Omega 2022, 7, 40241−40256

which the charges of the atoms (obtained by population analysis) replace the electron densities in the last three equations.[60] This is a simpler but efficient way to calculate these reactivity descriptors, widely employed for organic molecules[54,61] and studies about selectivity in organic reactions,[62] which is the main goal of this work. All calculations cited here were performed using the Gaussian 09 package.

3. RESULTS AND DISCUSSION

3.1. Chemistry. The aminoquinone compounds **9a−9g** were prepared using the synthetic sequence illustrated in Scheme 3. Bromination of vanillin with molecular bromine in acetic acid gave the 3-bromo derivative **12** in good yield.[63] The brominated derivative was transformed into 2-bromo-6-methoxy-1,4-benzoquinone **6** by reaction with an aqueous solution of 30% hydrogen peroxide in basic medium.[64] It was observed that the reaction of aniline **7a** and its related analogues **7b−7g** with the benzoquinone **6** resulted in the corresponding Michael addition products, 3-bromo-5-methoxy-2-aminoquinone derivatives **9a−9g**, in yields ranging from 35 to 57%. All experiments were conducted using an excess of the nucleophilic substances. This reaction also gave an unknown product insoluble in organic solvents, which upon thin-layer chromatography (TLC) analysis showed a retention factor similar to that of compounds **9a−9g**. The instability of quinone **6** in organic and aqueous solutions at room temperature and the difficulty in isolating the derivatives **9a−9g** from a mixture of substances by column chromatographic technique led to decreased yields.

In contrast, the nucleophilic substitution of phenol **13a** and its derivatives **13b−13d** in basic medium at room temperature occurred preferentially at the C2 position of benzoquinone **6** to generate 2-methoxy-6-aryloxy-compounds **10a−10d** in yields ranging from 29 to 47%. This reaction was problematic to separate.

The structures of compounds **9a−9g** and **10a−10d** were established based on one- and two-dimensional ^{1}H and ^{13}C NMR experiments and mass spectrometry (MS) analysis. The monocrystal X-ray diffraction analysis of compound **9b** (Figure 3) was performed to definitively prove the exact structure of

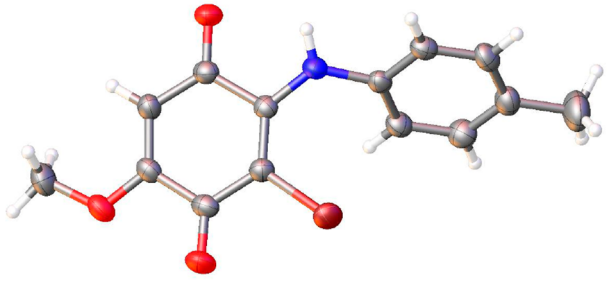

Figure 3. Asymmetric unit representation of the aminoquinone derivative **9b**. Displacement ellipsoids are drawn at the 50% probability level.

the unexpected product. Based on the X-ray crystallographic analysis, the molecular structure was confirmed, and the result showed that the amine group was incorporated exactly in the C-3 position of the quinonoid ring of **6**, with the permanence of halogen in the molecule, corroborating with the information obtained by ^{1}H and ^{13}C NMR techniques.

3.2. Thermodynamic Investigation. Figure S5 shows the ωB97X-D/6-31G(d,p)-LANL2DZ scan results, which point to the best orientation of the CH_3 group (all carbon atoms are coplanar). It is possible to see that the planar structures are related to the lowest energies (3.8 kcal·mol^{-1} more stable than the other local minima). All other intermediates, transition states, and products that will be discussed here were constructed using this spatial orientation ($\varphi_{C1C6OCH_3} = \pm 180°$).

The geometries of the reactants and products derived from the unsubstituted phenolate/aniline (with label "a") were optimized at the ωB97X-D/6-31G(d,p)-PCM water or acetonitrile, and harmonic frequencies were calculated at the same level of theory, in order to estimate the free energy of the reactions represented by Scheme 2. To obtain more accurate results, the geometries of all species were reoptimized, and vibrational frequencies were calculated, improving the basis set to a triple-ζ quality (6-311+G(2d,p)). Our results with 6-31G(d,p) and 6-311+G(2d,p) basis sets are shown in Figure 4.

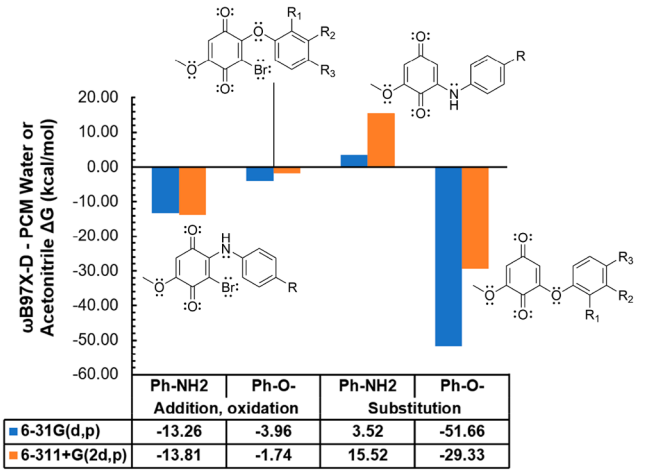

Figure 4. ΔG_r calculated (in kcal/mol) at ωB97X-D/6-31G(d,p) and 6-311+G(2d,p)-LANL2DZ-PCM water (reaction with Ph-NH_2) and acetonitrile (reaction with Ph-O^-).

They strongly point toward a thermodynamic preference for the substitution product when phenolate is the nucleophile, in line with experimental observations. Our computed values suggest that the corresponding substitution reaction with aniline is not spontaneous due the positive ΔG_r values. For the products from the conjugate addition/oxidation mechanisms, the Gibbs free energy variation for both nucleophiles (Ph-NH_2 and Ph-O^-) is negative, but the reaction is almost 4 times more exergonic using aniline than phenolate. A relevant experimental point should be highlighted: the substitution product with aniline may have been formed in very low quantities (in line with the thermodynamic data), but it could not be isolated and characterized.

The increase of the basis set maintained the same trends in thermodynamic results for the addition/oxidation mechanisms but caused significant differences in the substitution mechanisms. It can be seen in Figure 4 that the substitution product for the reaction with aniline is thermodynamically unfavorable (positive value of ΔG_r). For the phenolate substitution mechanism, on the other hand, the value of ΔG_r became less negative, more consistent with organic reactions of this nature. The fact that the thermodynamically favored products were from the substitution mechanism (for phenolate) and

https://doi.org/10.1021/acsomega.2c04607
ACS Omega 2022, 7, 40241−40256

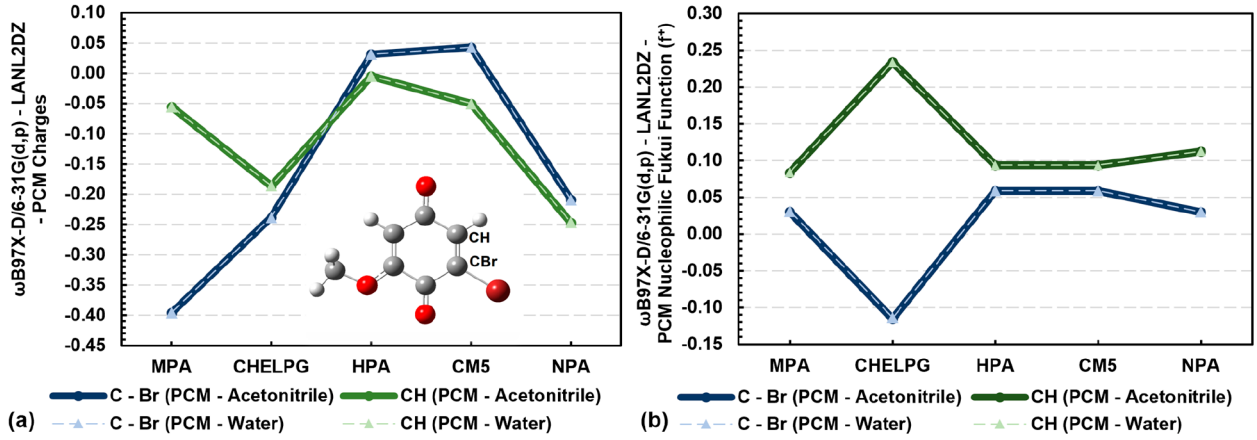

Figure 5. ωB97X-D/6-31G(d,p)-LANL2DZ-PCM water and acetonitrile Mulliken (MPA), ESP (CHELPG), Hirshfeld (HPA), CM5 and natural (NPA) (a) charges and (b) nucleophilic Fukui function for both C2−Br and C3−H carbon atoms.

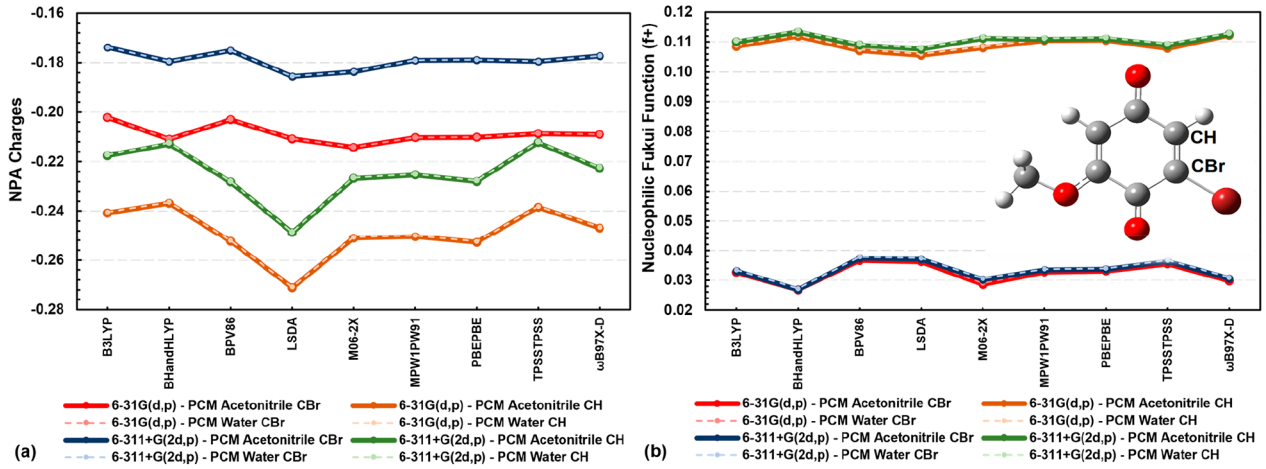

Figure 6. (a) CH and CBr natural (NPA) partial charges and (b) condensed nucleophilic Fukui function (f^+) calculated using B3LYP, BhandHLYP, BPV86, LSDA, M06-2X, MPW1PW91, PBEPBE, and ωB97X-D functionals combined with 6-31G(d,p) and 6-311+G(2d,p) basis sets, LANL2DZ pseudopotential, and PCM to consider the solvent acetonitrile and water effects.

addition/oxidation mechanism (for aniline) is totally in accordance with what was observed experimentally.

To verify the effect of the exchange of solvents on the spontaneity of the reactions represented by the global equations of Scheme 2, ωB97X-D/6-31G(d,p)-LANL2DZ-PCM ΔG_r values were calculated for aniline in acetonitrile and phenolate in water, with the values shown in Figure S6. It can be noted that the exchange of solvents turned all values more negative but did not affect the conclusion for the preferred mechanism for each nucleophile, which indicates that the difference in reactivity is a consequence of the interaction between the pair of reagents itself and not the solvent used.

3.3. Molecular and Kinetic Investigation. The mechanisms presented in Figures S1−S4 show that the formation of the different products depends on the nucleophilic attack at the C2 or C3 position of compound **6** by a variety of amines and phenoxide ions. This nucleophilic attack is a consequence of the interactions between molecules and atoms, which suggests the importance of the prediction of atomic and molecular properties, such as atomic partial charges and molecular orbitals. The ωB97X-D/6-31G(d,p)-LANL2DZ-PCM water or acetonitrile partial charges of the C2 (C−Br) and C3 (C−H), using different models, are shown in Figure 5 as well as the nucleophilic Fukui function (f^+). As one can see in Figure 5a, the partial charges are not significantly affected by the change in the simulated solvent but, rather, by the population analysis method used to calculate them, and, as mentioned before, the two most accurate charge models (CHELPG and NPA) produce similar charges. This figure also indicates a similar partial charge of the C2 and C3 atoms of **6**, which can contradict the common intuition of thinking that halogenated carbon is more positive than hydrogenated carbon. The similarities between the partial charges of these carbons can be understood by the small electronegativity difference between the bromine atom and the sp^2 carbon atom.[65] Although all charge models were used to calculate the nucleophilic Fukui function (f^+), as shown in Figure 5b, only the NPA model was used in further discussions and future calculations in other levels of theory.

Figure 6 shows the results of NPA charges and f^+, computed with several functionals combined with 6-31G(d,p) and 6-311+G(2d,p) basis sets. As expected, by the observation of the NPA charges, both carbon atoms have similar values for f^+, which indicate that the nucleophilic attack in both carbon atoms is feasible from a molecular point of view.

https://doi.org/10.1021/acsomega.2c04607
ACS Omega 2022, 7, 40241−40256

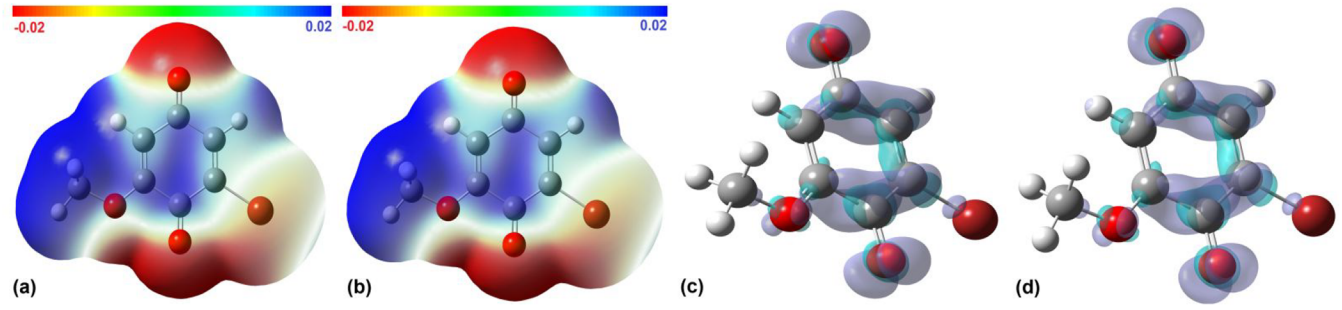

Figure 7. ωB97X-D/6-31G(d,p)-LANL2DZ electrostatic potential maps (isovalue = 0.0004) of the 1,4-benzoquinones in (a) PCM-water and (b) PCM-acetonitrile. The ωB97X-D/6-31G(d,p)-LANL2DZ nucleophilic Fukui function grid (isovalue = 0.004) is also represented in (c) PCM-water and (d) PCM-acetonitrile (positive values in purple and negatives in turquoise).

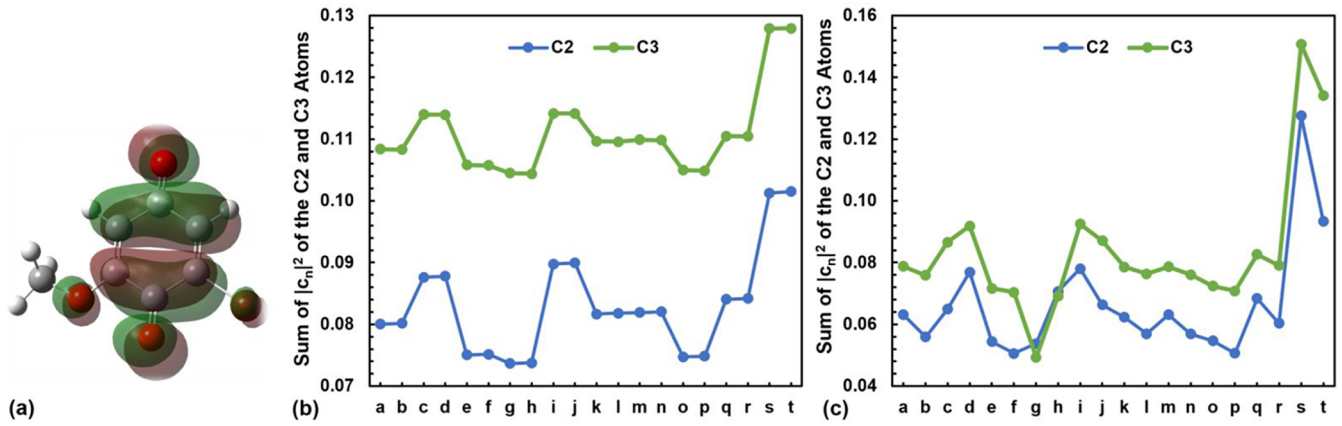

Figure 8. (a) ωB97X-D/6-31G(d,p)-LANL2DZ LUMO orbital (isovalue = 0.02) of the substrate in PCM-water and acetonitrile. Contribution of the atomic orbitals from C2 and C3 to the LUMO orbital by comparing the $|c_i|^2$, where c_i are the coefficients in the linear combinations of the atomic orbitals considered in the (b) 6-31G(d,p) and (c) 6-311+G(2d,p) basis sets. Functionals and solvents used in the PCM model: a (B3LYP-water), b (B3LYP-acetonitrile), c (BHandHLYP-water), d (BHandHLYP-acetonitrile), e (BPV86-water), f (BPV86-acetonitrile), g (LSDA-water), h (LSDA-acetonitrile), i (M06-2X-water), j (M06-2X-acetonitrile), k (MPW1PW91-water), l (MPW1PW91-acetonitrile), m (PBE1PBE-water), n (PBE1PBE-acetonitrile), o (TPSSTPSS-water), p (TPSSTPSS-acetonitrile), q (ωB97X-D-water), r (ωB97X-D-acetonitrile), s (MP2-water), and t (MP2-acetonitrile).

To get a visual representation of the properties mentioned so far (nucleophilic Fukui functions and partial charges), the electrostatic potential map and the condensed nucleophilic Fukui function were generated, and the surfaces are shown in Figure 7. Corroborating the last observations, the surfaces indicate that the C2 and C3 atoms have a similar tendency in receiving nucleophilic attacks; that is, the molecular properties described here point to a possibility of the formation of products with new groups in atoms C2 and C3. The calculated reactivity and electrostatic parameters do not show a preference for the nucleophilic attack to occur at C2 or C3, which corroborates the experimental observation of obtaining products with substituents on both carbons. Figure 7 also allows us to see that the changing of the solvent used in the PCM model does not affect electrostatic or reactivity trends.

Besides electrostatic features in the regiodivergent reaction of 2-bromo-1,4-quinones, we also attempted to rationalize the preferential formation of one product over another by molecular orbitals analysis. The first characteristic to be analyzed is the shape of the LUMO (particularly the π^*_{C2-C3}) orbital of the substrate in water and acetonitrile. Figure 8a shows this orbital (a π orbital with a high contribution of the p_z atomic orbitals), calculated at ωB97X-D/6-31G(d,p)-LANL2DZ-PCM-water and acetonitrile using the optimized structures. C2 and C3 atoms showed similar probability densities, which points to the possibility of the HOMO from the nucleophile interacting with any of the electrophilic sites in a similar manner. In addition, varying the implicitly simulated solvent does not affect the LUMO shape of the substrate. Figure 8b,c shows the sum of $|c_i|^2$ (linear coefficients used to construct the molecular orbital) calculated in several functionals and using the 6-31G(d,p) and 6-311+G(2d,p) basis sets. The values indicate a higher contribution of the C3 (C−H) atom than the C2 (C−Br) for the LUMO, suggesting that orbital interactions might be relevant to the conjugate addition/oxidation mechanism.

The atomic and molecular results discussed so far point to the inefficiency of common reactivity indices in describing the regiodivergence of 4-bromo-1,2-quinone reactions with phenolates and anilines, which requires further and more detailed investigations of the interaction between molecules, the spontaneity of the reaction (discussed thermodynamically in the section 3.2), and kinetics of the rate-determining step, as will be presented next.

Since most steps in the mechanisms represented in Figures S1−S4 consist of protonation and deprotonation processes of intermediates, the most important step of each mechanism is associated with the nucleophilic attack (the first step of each reaction route). Therefore, the species present in the first steps of Figures S1−S4 were reoptimized at the ωB97X-D/6-

https://doi.org/10.1021/acsomega.2c04607
ACS Omega 2022, 7, 40241−40256

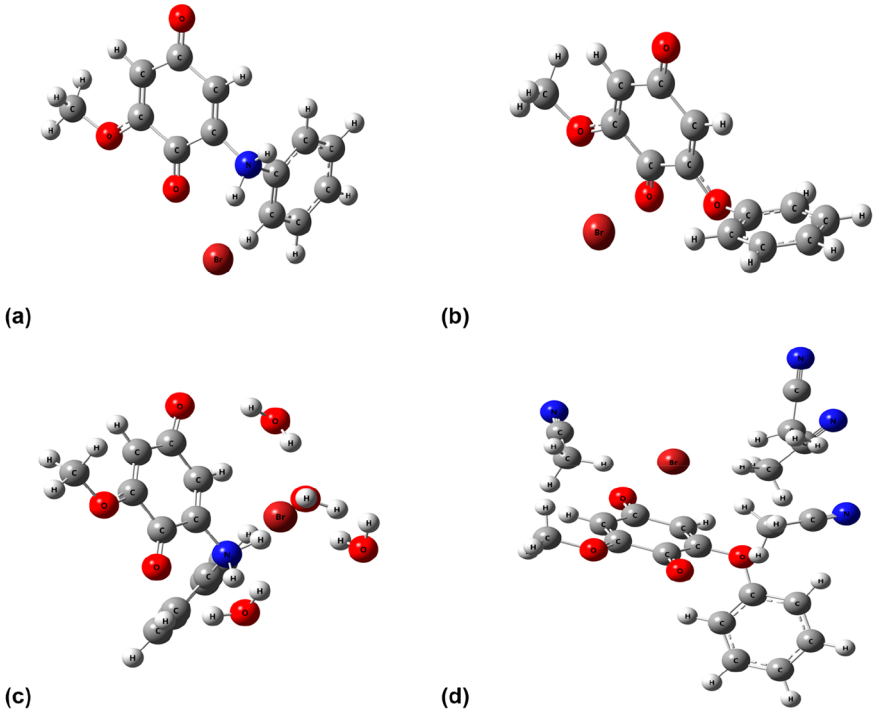

Figure 9. ωB97X-D/6-31G(d,p)-LANL2DZ-PCM optimized structures for the intermediates in the first steps of Figures S1−S4, using (a, b) the PCM approach and (c, d) PCM + four explicit solvent molecules.

Scheme 4. New Substitution Mechanisms, Proposed after the Optimization of the Intermediates of the First Steps Shown in (a) Figure S1 and (b) Figure S2

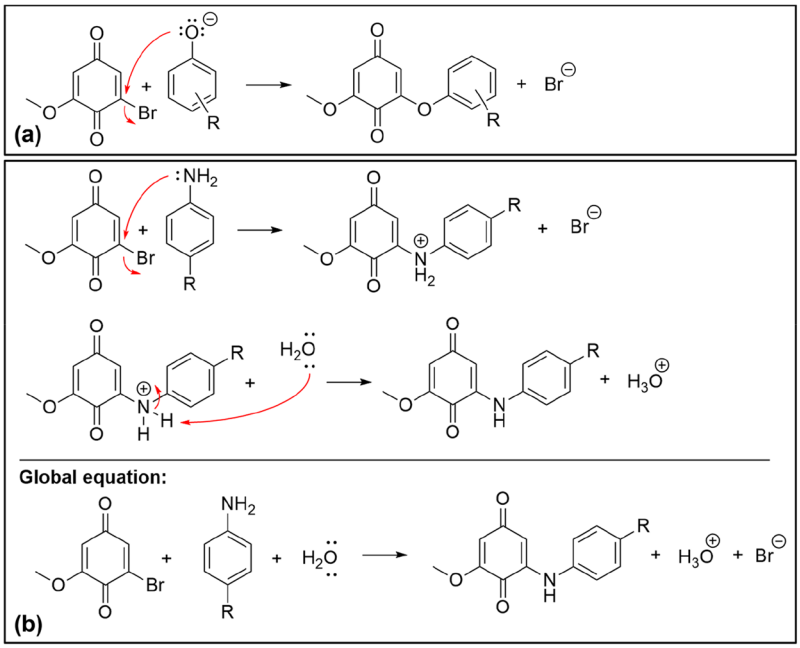

31G(d,p)-LANL2DZ−PCM-water or acetonitrile theory level and were characterized as true minimum energy points on the potential energy surface (PES) by the absence of imaginary frequencies. For the substitution mechanisms, the first intermediate consists of the nucleophile molecule connected to the C2 atom. We attempted to locate the intermediate, but optimization yielded the product complex, with the departure of the bromine atom as leaving group, as shown in Figure 9a,b. It suggests that the substitution reaction occurs concertedly (like the S_N2 mechanism, e.g.). To verify the existence of this cationic intermediate on the PES related to the substitution reaction mechanism, we explicitly modeled water solvent molecules (H_2O and CH_3CN) placed in suitable sites that allow the formation of hydrogen bonds. It can be seen, from Figure 9c, that the optimized structure of the intermediate present water molecules establishing hydrogen bonds with the partial negatively charged oxygen atom O1 and protonated nitrogen from aniline. It can be noticed that none of the

https://doi.org/10.1021/acsomega.2c04607
ACS Omega 2022, 7, 40241−40256

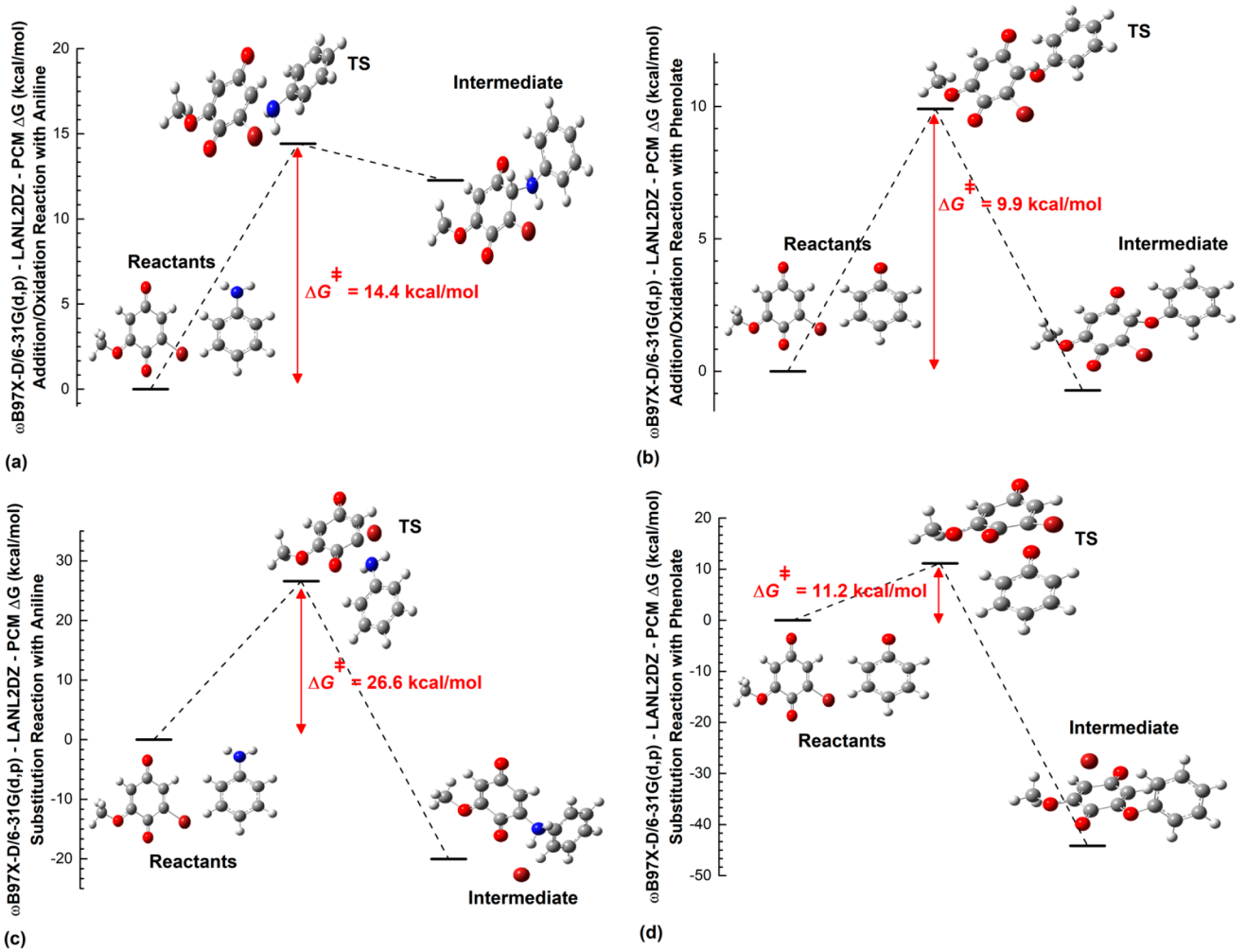

Figure 10. Relative Gibbs free energies (in kcal·mol^{-1}) between the chemical species involved in the first step of the mechanisms represented in Figures (a) S1, (b) S2, (c) S3, and (d) S4, calculated at the ωB97X-D/6-31G(d,p)-LANL2DZ-PCM water or acetonitrile.

strategies adopted to keep the halogen in the intermediate was successful; that is, optimizing the geometries in a conventional way, freezing coordinates, or positioning explicit solvent molecules lead to the same type of intermediate (with the elimination of the bromine atom), pointing to the possibility that nucleophilic attack on the sp^2 carbon and elimination of the halogen occur in the same step. The proposed substitution mechanisms, based on these results and different from those presented in Figures S1 and S2, are shown in Scheme 4.

In addition to the substrate/nucleophile molecular pairs and intermediates, the TSs associated with these nucleophilic attacks were also optimized at the same level of theory and were characterized as first-order saddle point of the PES, due to the presence of only one imaginary frequency, whose vibration involves breaking and formation of the chemical bond with the substrate. The energy diagrams for the nucleophilic attack steps with the optimized geometries of the species are shown in Figure 10, along with the energy barriers. It can be seen, from Figure 10a,c, that the first step of the substitution mechanism with aniline presents an energy barrier much higher than the corresponding value in the conjugate addition/oxidation mechanism, which indicates a kinetic preference for the addition/oxidation product. On the other hand, a comparison of Figure 10b,d reveals that, for the reaction with phenolates, both mechanisms present the first step with similar energy barriers; that is, from the kinetic point of view, both products are feasible. The kinetic and thermodynamic results show that, for anilines, the addition/oxidation product has a thermodynamic and kinetic preference to be formed. For phenolate, the substitution product has an expressive thermodynamic preference compared to the conjugate addition/oxidation product (see Figure 4).

The HOMO of the transition states arises from the interaction and donation of electron density from the HOMO of the nucleophile to the LUMO of the substrate. The HOMO orbital of the TS for the substitution mechanism with phenolate is shown in Figure 11a. This transition state has an imaginary frequency equal to −378.9 cm^{-1}, and it is possible to clearly see an HOMO−LUMO interaction. A similar behavior is observed for 10 TS structures for a substitution mechanism with aniline (imaginary frequency equals −317.9 cm^{-1}) and for the addition/oxidation mechanism with aniline (imaginary frequency equal to −302.3 cm^{-1}), shown in Figure 11b,c, respectively. However, when we turn our attention to the TS for the addition/oxidation mechanism with phenolates (imaginary frequency equal to −43.6 cm^{-1}), the interaction between the HOMO and LUMO orbitals shows a strong contribution of the C4 and C5 atoms of the substrate, different from the equivalent and pronounced TS shown in Figure 11c. For this TS, eight

https://doi.org/10.1021/acsomega.2c04607
ACS Omega 2022, 7, 40241−40256

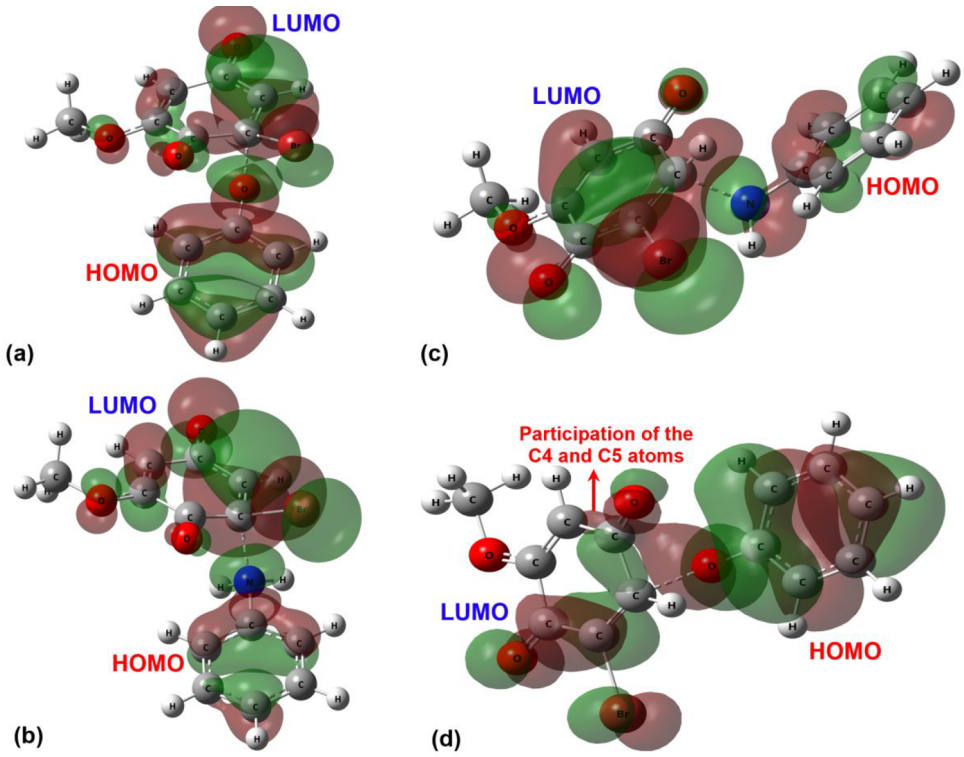

Figure 11. ωB97X-D/6-31G(d,p)-LANL2DZ-PCM water or acetonitrile HOMO orbital of the transition states for the first steps of the mechanisms indicated in Figures (a) S1, (b) S2, (c) S3, and (d) S4.

attempts were made (among changing the relative position of the molecules, freezing coordinates, and scan calculations), and all of them gave the nucleophilic attack in the C4 atom. The closest and similar transition state to that shown in Figure 11c that could be obtained was the one shown in Figure 11d but with a less negative imaginary frequency and weak approximation between the C3 atoms and the oxygen of the phenolate, which indicates that phenolate nucleophilic attack at the C2 atom (as shown in Figure 11a) is much more likely to occur than at the C3 atom (Figure 11d). The absence of the affinity between the C3 atom and the oxygen from the phenolate explains the almost zero energy difference indicated in Figure 10b between the reactants and the intermediate; that is, the separated and connected systems are very similar thermodynamically and must be associated with the preference of the substitution product over the addition/oxidation. A summary of the geometric and vibrational data of the TS is shown in Table 1, which contains the distances between ArO-C and ArN-C atoms (involved in the nucleophilic attack), calculated at ωB97X-D/6-31G(d,p)-LANL2DZ-PCM. The data indicate the greater distance ArO···C for the addition/oxidation TS, consistent with the lack of affinity between the C3 and the nucleophile.

Table 1. Imaginary Frequencies and Distances between ArO···C and ArN···C Atoms in the Nucleophilic Attack, Calculated at ωB97X-D/6-31G(d,p)-LANL2DZ-PCM for the Transition States of the First Steps of the Mechanisms Represented in Figures S1−S4

Orientation	Mechanism	Imaginary frequency (cm^{-1})	ArO···C or ArN···C bond length (Å)
Phenolate	Substitution	−378.9	1.81
	Addition/oxidation	−41.6	2.10
Aniline	Substitution	−317.9	1.75
	Addition/oxidation	−302.3	1.82

To investigate the strength of the interactions between the orbitals of the atoms and the donation of electron density, NBO analyses were done at the ωB97X-D/6-31G(d,p)-LANL2DZ-PCM level for the transition states of the four mechanisms considered in this work, with the results shown in Table 2. It was observed, in the TS for the addition/oxidation with aniline, a strong interaction between the lone pair of the nitrogen atom from the aniline and the π^*_{C2C3} orbital of the substrate, with $E(2)$ = 180.6 kcal·mol^{-1}, characteristic of a nucleophilic attack. On the other hand, for the substitution mechanism with the same nucleophile, the most remarkable donation observed is the interaction of the σ_{NH} from the amino group to the σ^*_{C2Br} with $E(2)$ = 1.2 kcal·mol^{-1}, without any character of a nucleophilic attack. As described above, the

Table 2. Second-Order Perturbation Theory Analysis of Fock Matrix in NBO Basis at ωB97X-D/6-31G(d,p)-PCM for the Transition States of the First Steps of the Mechanisms Represented in Figures S1−S4

Orientation	Mechanism	Donor	Acceptor	$E(2)$ (kcal·mol^{-1})
Phenolate	Substitution	Lone pair (O)	π^*_{C2C3}	138.35
	Addition/oxidation	Lone pair (O)	π^*_{C2C3}	44.07
Aniline	Substitution	σ_{NH}	σ^*_{C2Br}	1.17
	Addition/oxidation	Lone pair (N)	π^*_{C2C3}	180.63

https://doi.org/10.1021/acsomega.2c04607
ACS Omega 2022, 7, 40241−40256

Table 3. Second-Order Perturbation Theory Analysis of Fock Matrix in NBO Basis, Relative Energies, and Geometrical Properties of the Hydrogen Bonds Calculated at ωB97X-D/6-31G(d,p)-PCM for the Molecular Pairs with NH···O1 and NH···O4 Orientations

Pair orientation	ΔE_{rel} (kcal/mol)	Interaction	Donor NBO(i)	Acceptor NBO(i)	$E(2)$ (kcal/mol)	d (Å)	θ (deg)
NH···O1	0.00	HB1	LP (O1)	σ^*_{NH}	4.66	2.1	161.5
		HB2		$\sigma^*_{CHortho}$	0.74	2.7	168.5
NH···O4	−2.8	HB1	LP (O4)	σ^*_{NH}	7.19	2.1	157.8
		HB2		$\sigma^*_{CHortho}$	0.19	2.6	134.5
		HB3		σ^*_{C3H}	3.03	2.4	138

transition state for the nucleophilic attack of the phenolate on atom C2 (substitution mechanism) showed a strong interaction between the electron pair of oxygen (nucleophile) and the π^*_{C2C3} orbital, with $E(2)$ = 138.4 kcal·mol^{-1}, characteristic of a nucleophilic attack. The transition state for the nucleophilic attack of the phenolate on atom C3 (addition/oxidation mechanism) presented an interaction between the electron pair of oxygen (nucleophile) and the π^*_{C2C3} orbital, with $E(2)$ = 44.1 kcal·mol^{-1}, weaker than the last one (substitution mechanism). All the results summarized in Table 2 agree with kinetic and thermodynamic predictions.

The shorter distances of the ArN···C atoms and the higher $E(2)$ values shown in Tables 1 and 2 indicate that there is a strong interaction between the quinone and the aniline. To investigate whether hydrogen bonds can contribute to the approximation of aniline in the vicinity of atom C3, two molecular pairs formed by the aniline and the quinone were optimized at the same level of theory used for the reactants: the first pair has the N−H···O1 orientation, and the other one has the N−H···O4 orientation. These geometries also passed through NBO calculations and NCI analysis, to characterize the interactions.

The relative energies and the geometric values of the hydrogen bonds and angles are shown in Table 3, which allows us to observe two hydrogen bonds in each pair: the NH···O1/O4 (named HB1) and CH_{orto}(aniline)···O1/O4 (named HB2), with similar lengths. Furthermore, the N−H···O4 orientation is 2.8 kcal/mol more stable than the N−H···O1 orientation, which indicates that the first one is more likely to be found than the second one (based on the Boltzmann population). The higher value for $E(2)$ also suggests that the N−H···O4 interaction is stronger than N−H···O1.

However, a third interaction (named HB3) can be identified in the N−H···O4 orientation, related to the C3−H···N approximation, with similar length to the hydrogen bonds cited here and can be associated with the extra stability of the molecular pair. The $E(2)$ value for this attraction is also coherent to that proposed by Li et al., which pointed out the existence of a C−H···O hydrogen bond, with $E(2)$ stabilization energy values close to 0.78 kJ·mol^{-1}, associated with the donation of electron density from the oxygen (lone pair) to the antibonding orbital (LP → σ^*_{CH})[66] of the receptor. The RDG scatter maps and NCI plots for the optimized molecular pairs are shown in Figure S7 and can give a visual representation of the interactions described here.

The data described here indicate that the stronger interactions in the NH···O4 orientation could explain the higher concentration of nucleophile molecules in the vicinity of the carbon 3, acting as a guide for the reactive site of the nucleophilic attack. However, to ensure that, it is necessary to perform the reaction with aniline in different solvents, varying the polarity and ability to form hydrogen bonds, which goes beyond the scope of this work but surely deserves future investigations; that is, the results on hydrogen bonds constitute only a theoretical indication but lack a complex experimental validation. The main results that differ between the two mechanisms presented here are the kinetic and thermodynamic data. The experimental synthesis of the aminoquinones reported here was performed in an aqueous solution due the higher yields obtained for reactions between quinones and amines using water as solvent, as reported by Yadav et al. in their green synthesis of aminoquinones in aqueous solution,[67] and difficulties in the experimental procedure (synthesis and separation of the product) should arise if the reaction is performed in other solvents.

4. CONCLUSIONS

This work aimed to describe, with thermodynamic, kinetic, and molecular arguments, the regiodivergent reactions of benzoquinone **6** with different nucleophiles: phenolates and anilines. Experimentally, the substitution product for the reaction with phenolates and the addition/oxidation product for the reaction with anilines were observed, which is corroborated by the theoretical free energies of the reactions.

The evaluation of energies of the species involved in the nucleophilic attack showed the kinetic preference of the addition/oxidation product for the reaction of **6** with aniline. For phenolates, on the other hand, both addition/oxidation and substitution mechanisms have similar energy barriers. The NBO analysis was carried out for the TS structures, showing that, for nucleophilic attacks N → C3 and O → C2, there is an electronic density donation, derived from the interaction between the pair of electrons of oxygen or nitrogen (from the nucleophile) and the π^*_{C2C3} orbital of the substrate, both with high NBO stabilization energy ($E(2)$ > 300 kcal·mol^{-1}), characteristic of an efficient nucleophilic attack. For TSs associated with nucleophilic attacks N → C2 and O → C3, interactions have much lower values of $E(2)$ and reveal an inefficient nucleophilic attack.

The calculation of partial charges using different models (MPA, CHELPG, HPA, CM5, and NPA) showed that carbon 3 (CH) of **6** presents a partial charge more positive than carbon 2 (CBr), which is consistent with the possibility of nucleophilic attack on both carbons (this trend did not change with the variation of base functions). The analysis of the molecular properties of **6** (LUMO, electrostatic potential maps, and the isosurface of the Fukui function) also indicated that there are no substantial differences between the reactivity characteristics of the C2 and C3 atoms of **6**; that is, both are proven susceptible to nucleophilic attack, but we pointed out that regiodivergence was correctly predicted by thermodynamic and kinetic data.

The characterization of the hydrogen bonds formed by an aniline molecule and the quinone indicates that the

https://doi.org/10.1021/acsomega.2c04607
ACS Omega 2022, 7, 40241−40256

intermolecular interaction can increase the concentration of nucleophile molecules around the C3 atom, but it deserves additional experimental verification, which requires a new synthesis using several solvents. Theoretical thermodynamic, kinetic, and molecular properties results provide support to experimental observations and enabled us to clarify in more detail the regiodivergence of the chemical reactions presented here.

5. EXPERIMENTAL SECTION

5.1. Chemistry. Infrared (IR) spectra were recorded on a PerkinElmer FT-IR, model 1600 series spectrophotometer in KBr pellets. NMR spectra were recorded on a Varian VNMRS 300 or 500 MHz spectrometer, in the specified solvents. Chemical shifts (δ) are reported in parts per million, and the coupling constants (J) are expressed in hertz. Through the signs of the integrations, the multiplicities were described as follows: s-simplet; d-doublet; m-multiplet, dd-double−doublet. Melting points were determined with Fisher-Johns Melting Point Apparatus instrument and are uncorrected. The high-resolution mass spectrum (HRMS) was performed on the Micromass Q-TOF (water) mass spectrometer.

The reactions were monitored by TLC performed on silica gel 60 (Merck) and revealed under ultraviolet light at 254 nm. The purification of the products was done by flash column chromatography Merck silica gel and preparative plate chromatography Merk silica gel 60 PF_{254}.

5.2. General Procedure for the Synthesis of 3-Bromo-4-hydroxy-5-methoxybenzaldehyde (12).[52] To a 50 mL round-bottom flask containing 6.7 mmol of vanillin **11** dissolved in 1.3 mL of glacial acetic acid was added a solution of 0.360 mL of molecular bromine dissolved in 2 mL of acetic acid. The reaction was kept under stirring and at room temperature for a period of 15 min. Subsequently, the reaction medium was treated with a saturated solution of sodium sulfite (6 mL), and the mixture obtained was vacuum filtered in a Büchner funnel. The solid was washed with portions of the $NaHSO_3$ solution and distilled water. The brominated vanillin **12** were purified by recrystallization from ethanol.

*3-Bromo-4-hydroxy-5-methoxybenzaldehyde (**12**).* White solid (yield 95%), mp: 212−214 °C; IR (KBr, ν cm^{-1}): 3279 (O−H), 2780 and 2848 (C<u>H</u>O), 1672 (C═O), 1287 and 1044 (C−O). NMR of ^1H (500.00 MHz, dimethyl sulfoxide (DMSO-d_6)) δ (ppm): 3,89 (1H, s, OC<u>H</u>$_3$); 7,41 (1H, d, J = 1,7 Hz, H-6); 7,69 (1H, d, J = 1,8 Hz, H-2); 9,76 (1H, s, C<u>H</u>O).

5.3. General Procedure for the Synthesis of 2-Bromo-6-methoxy-1,4-benzoquinone (6).[53] To a 50 mL round-bottom flask were added 3.5 mmol of bromovanillin **12** and 4.4 mL of 1 M aqueous potassium hydroxide solution. The mixture was allowed to stir at room temperature for 10 min. Subsequently, 9.8 mL of a 3% aqueous solution of hydrogen peroxide was added. The reaction was kept under stirring at room temperature for 15 min in an ultrasound bath at 40 °C for 2 h. After 2 h of reaction, the organic phase was extracted with ethyl acetate solvent, treated with anhydrous sodium sulfate, and then concentrated under reduced pressure. After concentration of the solvent under reduced pressure a solid was obtained, which was treated with hot *n*-hexane. The obtained filtrate was concentrated under reduced pressure, yielding 2-bromo-6-methoxy-1,4-benzoquione (**6**).

*2-Bromo-6-methoxy-1,4-benzoquinone (**6**).* Yellow solid (yield 65%), mp: 139−143 °C, mp: 212−214 °C; IR (KBr, ν cm^{-1}): 1696 and 1631(C═O), 1230 (C−O). NMR of ^1H (300,00 MHz, DMSO-d_6) δ (ppm): 3,81 (3H, s, C<u>H</u>$_3$); 6,13 (1H, d, J = 2,3 Hz, H-5); 7,32 (1H, d, J = 2,3 Hz, H-3).

5.4. General Procedure for the Synthesis of Amino-cyclohexa-2,5-diene-1,4-dione (9a−9g). To a round-bottom flask, 1 mmol of 2-bromo-6-methoxy-1,4-benzoquinone (**6**), 1.3 mmol of aniline (**7a−7g**), and 10 mL of water were added. The reaction was left under irradiation in an ultrasound bath for 3 h. Posteriorly, the mixture was filtrated in Buchner funnel, and the precipitate obtained was washed with distilled water. The phenylamino-1,4-benzoquinone derivatives **9a−9g** were purified by column chromatography on silica gel using a 9:1 *n*-hexane/ethyl acetate mixture as eluent.

*3-Bromo-5-methoxy-2-(phenylamino)cyclohexa-2,5-diene-1,4-dione (**9a**).* Violet solid (yield 49%), mp: 178−180 °C; IR (KBr, ν cm^{-1}): 3239 (N−H); 1650 and 1626 (C═O), 1237 and 1009 (C−O). ^1H NMR (300.00 MHz, DMSO-d_6) δ (ppm): 3.85 (s, 3H, OC<u>H</u>$_3$); 6.10 (s, 1H, H-6); 7.08−7,18 (m, 3H, H-2′/H-4′/H-6′); 7.28−7,34 (m, 2H, H-3′/H-5′). ^{13}C NMR (75.0 MHz, DMSO-d_6) δ (ppm): 57.0 (OCH_3); 99.5 (C3); 103.8 (C6); 124.7 (C2′/C6′); 125.0 (C4′); 127.9 (C3′/C5′); 138.1 (C1′); 143.7 (C2); 160.5 (C5); 173.5 (C4); 181.2 (C1). HRMS (M^+): m/z calculated for $C_{13}H_{10}BrNO_3$: 306.9844; found: 306.9830.

*3-Bromo-2-(4-methylphenylamino)-5-methoxy-cyclohexa-2,5-diene-1,4-dione (**9b**).* Purple solid (yield 47%), mp: 188−189 °C; IR (KBr, ν cm^{-1}): 324 2 (N−H); 1652 and 1621 (C═O); 1236 and 1003 (C−O). ^1H NMR (300.00 MHz, DMSO-d_6) δ (ppm): 2.28 (s, 3H, C4′-CH_3); 3.84 (s, 3H, OC<u>H</u>$_3$); 6.08 (s, 1H, H-6); 7.00 (d, 2H, J = 9.0 Hz, H-2′/H-6′); 7.31 (d, 2H, J = 9.0 Hz, H-3′/H-5′). ^{13}C NMR (75.0 MHz, DMSO-d_6) δ (ppm): 20.4 (C4′-<u>C</u>H$_3$); 56.9 (OCH_3); 98.5 (C3); 103.6 (C6); 124.8 (C2′/C6′); 128.3 (C3′/C5′); 134.3 (C1′); 135.3 (C4′); 143.6 (C2); 160.6 (C5); 173.2 (C4); 181.2 (C1). HRMS (M^+): m/z calculated for $C_{14}H_{12}BrNO_3$: 321.0001; found: 321.9917.

*3-Bromo-5-methoxy-2-((4-methoxyphenyl)amino)-cyclohexa-2,5-diene-1,4-dione (**9c**).* Purple solid (yield 47%), mp: 186−188 °C; IR (KBr, ν cm^{-1}): 3236 (N−H); 1649 and 1625 (C═O), 1234 and 1011 (C−O). ^1H NMR (300.00 MHz, DMSO-d_6) δ (ppm): 3.76 (s, 3H, C4′-O<u>C</u>H$_3$); 3.84 (s, 3H, C6-OC<u>H</u>$_3$); 6.07 (s, 1H, H-6); 6.88 (d, 2H, J = 9.0 Hz, H-2′/H-6′); 7.06 (d, 2H, J = 9.0 Hz, H-3′/H-5′). ^{13}C NMR (75.0 MHz, DMSO-d_6) δ (ppm): 55.2 (C4′-O<u>C</u>H$_3$); 56.9 (C5-OCH_3); 97.2 (C3); 103.4 (C6); 113.1 (C2′/C6′); 126.6 (C3′/C5′); 130.7 (C1′); 143.7 (C2); 157.0 (C4′); 160.7 (C5); 173.1 (C4); 181.1 (C1). HRMS (M^+): m/z calculated for $C_{14}H_{12}BrNO_4$: 336.9950; found: 336.9942.

*3-Bromo-5-methoxy-2-((4-chlorophenyl)amino)-6-methoxycyclohexa-2,5-diene-1,4-dione (**9d**).* Purple solid (yield 55%), mp: 210−212 °C; IR (KBr, ν cm^{-1}): 3157 (N−H); 1660 and 1645 (C═O); 1228 and 1007 (C−O). ^1H NMR (300.00 MHz, DMSO-d_6) δ (ppm): 3.85 (s, 3H, OCH_3); 6.12 (s, 1H, H-6); 7.12 (d, 2H, J = 8.2 Hz, H-2′/H-6′); 7.35 (d, 2H, J = 8.2 Hz, H-3′/H-5′). ^{13}C NMR (75.0 MHz, DMSO-d_6) δ (ppm): 57.0 (OCH_3); 100.6 (C3); 104.0 (C6); 126.0 (C2′/C6′); 127.8 (C3′/C5′); 128.7 (C1′); 137.2 (C4′); 143.5 (C2); 160.3 (C5); 173.6 (C4); 181.2 (C1). HRMS (M^+):m/z calculated for $C_{13}H_9BrClNO_3$: 340.9454; found: 341.9363.

*3-Bromo-5-methoxy-2-((4-fluorophenyl)amino)-6-methoxycyclohexa-2,5-diene-1,4-dione (**9e**).* Purple solid (yield 47%), mp: 158−160 °C; IR (KBr, ν cm^{-1}): 3239 (N−H); 1652 and 1625 (C═O); 1999 and 1005 (C−O). ^1H NMR

https://doi.org/10.1021/acsomega.2c04607
ACS Omega 2022, 7, 40241−40256

(300.00 MHz, DMSO-d_6) δ (ppm): 3.89 (s, 3H, OCH_3); 5.88 (s, 1H, H-6); 7.00−7,10 (m, 4H, H-2′/H-3′/H-4′/H-5′/H-6′); 7.71 (s, 1H, N−H). ^{13}C NMR (75.0 MHz, DMSO-d_6) δ (ppm): 57.2 (OCH_3); 98.7 (C3); 103.1 (C6); 115.5 (C3′/C5′, d, J_{CF} = 22.68 Hz); 127.5 (C2′/C6′, d, J_{CF} = 8.8 Hz,); 132.8 (C1′, d, J_{CF} = 2.5 Hz); 142.7 (C2); 161.1 (d, J_{CF} = 248 Hz, C4′); 161.5 (C5); 174.2 (C4); 181.3 (C1). HRMS (M^+): m/z calculated for $C_{13}H_9BrFNO_3$: 324.9750; found: 324.9759.

*3-Bromo-5-methoxy-2-((4-nitrophenyl)amino)cyclohexa-2,5-diene-1,4-dione (**9f**).* Purple solid (yield 29%), mp: 250−251 °C; IR (KBr, ν cm^{-1}): 3276 (N−H); 1664 and 1644 (C═O); 1578 and 1338 (NO_2); 1236 and 999 (C−O). ^{1}H NMR (300.00 MHz, DMSO-d_6) δ (ppm): 3.86 (s, 3H, OCH_3); 6.18 (s, 1H, H-6); 7.21 (d, 2H, J = 9.0 Hz, H-2′/H-6′); 8.15 (d, 2H, J = 9.0 Hz, H-3′/H-5′), 9.56 (1H, s, N−H). ^{13}C NMR (75.0 MHz, DMSO-d_6) δ (ppm): 57.2 (OCH_3); 104.9 (C6); 108.7 (C3); 121.8 (C2′/C6′); 123.9 (C3′/C5′); 142.0 (C1′); 143.0 (C2); 145.5 (C4′); 159.8 (C5); 174.2 (C4); 181.2 (C1). HRMS (M^+): m/z calculated for $C_{13}H_9BrN_2O_5$: 351.9695; found: 352.9623.

*3-Bromo-5-methoxy-2-((4-bromophenyl)amino)-6-methoxycyclohexa-2,5-diene-1,4-dione (**9g**).* Purple solid (yield 49%), mp: 181−183 °C; IR (KBr, ν cm^{-1}): 3207 (N−H); 1663 and 1665 (C═O); 1215 and 1002 (C−O). ^{1}H NMR (300.00 MHz, DMSO-d_6) δ (ppm): 3.89 (s, 3H, OCH_3); 5.90 (s, 1H, H-6); 6.95 (d, 2H, J = 9.0 Hz, H-2′/H-6′); 7.46 (d, 2H, J = 9.0 Hz, H-2′/H-6′); 7.67 (s, 1H, N−H). ^{13}C NMR (75.0 MHz, DMSO-d_6) δ (ppm): 57.2 (OCH_3); 99.9 (C3); 103.3 (C6); 119.7 (C4′); 126.8 (C2′/C6′); 131.7 (C3′/C5′); 142.3 (C2); 161.4 (C5); 174.2 (C4); 181.3 (C1). HRMS (M^+):m/z calculated for $C_{13}H_9Br_2NO_3$: 387.0235; found: 386.8930.

5.5. General Procedure for the Synthesis of Phenoxy-cyclohexa-2,5-diene-1,4-dione derivatives (10a−10d). To a 50 mL round-bottom flask were added 0.35 mmol of the properly substituted phenol (**8a−8d**) and 5 mL of acetonitrile. Then 1.05 mmol of K_2CO_3 was added, and the reaction medium was kept under continuous stirring for 1 h at room temperature. After this, 0.35 mmol of 2-bromo-6-methoxy-cyclohexa-2,5-diene-1,4-dione (**6**) in 4 mL of acetonitrile was added slowly and stirred for 3 h. Monitoring the reaction by TLC was performed using hexane/ethyl acetate (7:3) as the eluent. The organic phase was extracted with ethyl acetate solvent, treated with anhydrous sodium sulfate, and then concentrated under reduced pressure. The derivatives **10a−10d** were purified by preparative plate chromatography using a 9:1 (v/v) hexane/ethyl acetate mixture as eluent.

*2-Methoxy-6-phenoxy-cyclohexa-2,5-diene-1,4-dione (**10a**).* Yellow solid (yield 48%), mp: 115−117 °C; IR (KBr, ν cm^{-1}): 1652 and 1624 (C═O). ^{1}H NMR (500.00 MHz, $CDCl_3$) δ (ppm): 3.86 (s, 3H, C2-OC$\underline{H}_3$); 5.65 (d, 1H, J = 2.5 Hz, H-3); 5.86 (d, 1H, J = 2.0 Hz, H-5); 7.08−7.10 (dd, 2H, J = 8.5 and 1.0 Hz, H-2′/H-6′); 7.30 (d, 1H, J = 8.5 Hz, H-4′); 7.42−745 (m, 2H, H-3′/H-5′). ^{13}C/APT NMR (125.0 MHz, $CDCl_3$) δ (ppm): 57.1 (C2−O$\underline{C}H_3$); 107.4 (C-3); 111.1 (C-5); 121.1 (C-2′/C-6′); 126.7 (C-4′); 130.5 (C-3′/C-5′); 152.8 (C-1′); 157.5 (C-2); 162.6 (C-6); 176.6 (C-4), 186.9 (C-1).

*2-(4-Formyl-2-methoxyphenoxy)-6-methoxy-cyclohexa-2,5-diene-1,4-dione (**10b**).* Red solid (yield 29%) mp: 130−132 °C. IR ((KBr, ν cm^{-1}): 2919 and 2850 (C−H); 1681 and 1639 (C═O). ^{1}H NMR (500.00 MHz, $CDCl_3$) δ (ppm): 3.84 (s, 3H, C2-OC$\underline{H}_3$); 3.86 (s, 3H, C-2′-OC$\underline{H}_3$); 5.54 (d, 2H, J = 2.0 Hz, H-3); 5.85 (d, 2H, J = 2.0 Hz, H-5); 7.24 (s, 1H, H-3′); 7.50 (dd, 1H, J = 8.0 and 2.0 Hz, H-6′); 7.51−7.52 (m, 1H, H-5′), 9.95 (s, 1H, C$\underline{H}$O). ^{13}C/APT NMR (125.0 MHz, $CDCl_3$) δ (ppm): 56.3 (C2′-O$\underline{C}H_3$); 56.8 (C2−O$\underline{C}H_3$); 107.5 (C-3); 111.3 (C-5); 111.7 (C-3′); 123.0 (C-5′); 125.2 (C-6′); 135.8 (C-4′); 141.9 (C-1′); 151.6 (C-2′); 153.4 (C-6); 157.7 (C-2); 171.6 (C-4); 171.8 (C-1); 190.7 (C$\underline{H}$O).

*2-Methoxy-4-(4-methoxyphenoxy)-cyclohexa-2,5-diene-1,4-dione (**10c**).* Yellow solid (yield 35%), mp: 122−124 °C; IR ((KBr, ν cm^{-1}): 1693 and 1641 (C═O). ^{1}H NMR (500.00 MHz, $CDCl_3$) δ ppm: 3.82 (s, 3H, C2-OC$\underline{H}_3$); 3.85 (s, 3H, C4′-OC$\underline{H}_3$); 5.64 (d, 1H, J = 2.0 Hz, H-3); 5.85 (d, 1H, J = 2.0 Hz, H-5); 6.93 (dd, 2H, J = 7.5 and 2,5 Hz, H-2′/H-6′); 7.00 (dd, 2H, J = 7.5 and 2.5 Hz, H-3′/H-5′). ^{13}C/APT NMR (125.0 MHz, $CDCl_3$) δ ppm: 55.8 (C-4′-O$\underline{C}H_3$); 56.7 (C2-O$\underline{C}H_3$); 107.4 (C-3); 110.8 (C-5); 115.4 (C-2′/C-6′); 122.0 (C-3′/C-5′); 157.6 (C-4′); 157.9 (C-2); 158.0 (C-1′); 159.9 (C-6); 183.4 (C-4); 187.0 (C-1).

*2-(4-Alyl-2-methoxyphenoxy)-6-methoxy-cyclohexa-2,5-diene-1,4-dione (**10d**).* Yellow solid (yield 32%), mp: 136−138 °C; IR (KBr, ν cm^{-1}): 1681 and 1642 (C═O); 1072 and 1026 (C−O). ^{1}H NMR (500.00 MHz, DMSO-d_6) δ (ppm): 3.41 (d, 2H, J = 6.5 Hz, C2′-OC$\underline{H}_3$); 3.77 (s, 3H, C2-OC$\underline{H}_3$); 3.81 (s, 3H, C2′-OC$\underline{H}_3$); 5.07−5.11 (m, 2H, CH−CH$_2$═C$\underline{H}_2$); 5.13−5.15 (m, 1H, C$\underline{H}$-CH$_2$═CH$_2$); 5.30 (d, 1H, J = 2.0 Hz, H-3); 6.00 (d, 1H, J = 2.0 Hz, H-5); 6.85 (dd, 1H, J = 8.0 and 2.0 Hz, H-5′); 7.04 (d, 1H, J = 2.0 Hz, H-3′); 7.09 (d, 1H, J = 8.0 Hz, H-6′). ^{13}C/APT NMR (125.0 MHz, DMSO-d_6) δ (ppm): 40.0 (C-3″); 55.7 (C2′-O$\underline{C}H_3$); 56.5 (C2−O$\underline{C}H_3$); 106.9 (C-3); 109.4 (C-5); 113.8 (C-3′); 115.9 (C-1″); 120.9 (C-6′); 121.5 (C-5′); 137.0 (C-2″); 138.8 (C-4′); 139.4 (C-1′); 150.0 (C-2′); 156.1 (C-6); 157.3 (C-2); 175.4 (C-4); 186.3 (C-1).

5.6. X-ray Diffraction Analysis. X-ray data collection and structure refinement. Single-crystal X-ray data for **9b** were collected on a Bruker D8 Venture diffractometer using graphite-monochromated Mo Kα radiation (λ = 0.710 73 Å) at 298 K. Data collection, cell refinement, and data reduction were performed with Bruker Instrument Service v4.2.2, APEX2,[68] and SAINT,[69] respectively. Absorption correction using equivalent reflections was performed with the SADABS program.[70] The structure solutions and full-matrix least-squares refinements based on F^2 were performed with the SHELX package[71,72] and were refined with fixed individual displacement parameters [Uiso\(H) = 1.2 Ueq (Csp^2 and C_{ar}) or 1.5 Ueq (Csp^3)] using a riding model. All nonhydrogen atoms were refined anisotropically. Crystallographic tables were constructed using Olex2.[73] X-ray crystallographic data in cif format are available and can be obtained free of charge via http://www.ccdc.cam.ac.uk/data_request/cif.

5.7. Crystal Data of 9b. $C_{14}H_{12}NO_3Br$ (M = 322.16 g/mol): monoclinic, space group $P2_1/c$, a = 7.1915(3)Å, b = 24.0597(11) Å, c = 7.7844(3) Å, β = 100.987(2)°, V = 1322.21(10) Å^3, Z = 4, T = 298.0 K, μ(Mo Kα) = 3.111 mm^{-1}, F(000) = 647.2, crystal size = 0.459 × 0.155 × 0.041 mm^3, D_{calc} = 1.6183 g/cm^3; of the 52 148 reflections measured (5.6° ≤ 2Θ ≤ 50.7°), 2420 were unique (R_{int} = 0.0493, R_{sigma} = 0.0144) and were used in all calculations. The final R_1 was 0.0348 ($I > 2\sigma(I)$), and $wR2$ was 0.0694 (all data).

■ ASSOCIATED CONTENT

Supporting Information

The Supporting Information is available free of charge at https://pubs.acs.org/doi/10.1021/acsomega.2c04607.

https://doi.org/10.1021/acsomega.2c04607
ACS Omega 2022, 7, 40241−40256

The generic mechanisms of the substitution and addition/oxidation reactions, the experimental IR and NMR spectra for the main substances exposed here (PDF)

AUTHOR INFORMATION

Corresponding Authors

Haroldo C. Da Silva − *Laboratório de Química Computacional e Modelagem Molecular, Departamento de Química Inorgânica, Universidade Federal Fluminense, Niterói 24020-150 RJ, Brazil*; Email: haroldocandal@id.uff.br

Wagner B. De Almeida − *Laboratório de Química Computacional e Modelagem Molecular, Departamento de Química Inorgânica, Universidade Federal Fluminense, Niterói 24020-150 RJ, Brazil*; orcid.org/0000-0003-0785-2284; Email: wbdealmeida@gmail.com

Anna C. Cunha − *Departamento de Química Orgânica, Universidade Federal Fluminense, Niterói 24020-141 RJ, Brazil*; Email: annacunha@id.uff.br

Authors

Talita O. C. Leite − *Faculdades Integradas Maria Thereza, Niterói 24020004 RJ, Brazil*

Searitha C. Rodrigues − *Departamento de Química Orgânica, Universidade Federal Fluminense, Niterói 24020-141 RJ, Brazil*

Beatriz L. C. De Carvalho − *Departamento de Química Orgânica, Universidade Federal Fluminense, Niterói 24020-141 RJ, Brazil*

Maria Tereza Martins − *Departamento de Química Orgânica, Universidade Federal Fluminense, Niterói 24020-141 RJ, Brazil*

Rodolfo G. Fiorot − *Departamento de Química Orgânica, Universidade Federal Fluminense, Niterói 24020-141 RJ, Brazil*

Flaviana R. F. Dias − *Departamento de Química Orgânica, Universidade Federal Fluminense, Niterói 24020-141 RJ, Brazil*; orcid.org/0000-0002-7069-9887

Vinícius R. Campos − *Departamento de Química Orgânica, Universidade Federal Fluminense, Niterói 24020-141 RJ, Brazil*

Vitor F. Ferreira − *Faculdade de Farmácia, Departamento de Tecnologia Farmacêutica, Programa de Pós-Graduação em Química, Universidade Federal Fluminense, Niterói 24241-000 RJ, Brazil*

Complete contact information is available at: https://pubs.acs.org/10.1021/acsomega.2c04607

Notes

The authors declare no competing financial interest.

ACKNOWLEDGMENTS

W.B.d.A. thanks the Conselho Nacional de Desenvolvimento Científico e Tecnológico (CNPq) for a research fellowship (Proc. No. 309269/2021-0) and Fundação Carlos Chagas Filho de Amparo à pesquisa do Estado do Rio de Janeiro (FAPERJ) for support (Proc. No. E-26/201.163/2021). H.C.d.S. thanks CNPq for a Ph.D. scholarship.

REFERENCES

(1) Zhang, Y.; Liu, J.; Chen, X.; Chen, C.-Y. O. Ubiquinol Is Superior to Ubiquinone to Enhance Coenzyme Q10 Status in Older Men. *Food Funct.* **2018**, *9* (11), 5653−5659.

(2) Ferreira, V. F.; de Carvalho, A. S.; Ferreira, P. G.; Lima, C. G. S.; de, C.; da Silva, F. Quinone-Based Drugs: An Important Class of Molecules in Medicinal Chemistry. *Med. Chem. (Los Angeles)* **2021**, *17* (10), 1073−1085.

(3) da Silva, R. E.; de Oliveira Silva Ribeiro, F.; de Carvalho, A. M. A.; Daboit, T. C.; Marinho-Filho, J. D. B.; Matos, T. S.; Pessoa, O. D. L.; de Souza de Almeida Leite, J. R.; de Araújo, A. R.; dos Santos Soares, M. J. Antimicrobial and Antibiofilm Activity of the Benzoquinone Oncocalyxone A. *Microb. Pathog.* **2020**, *149*, 104513.

(4) Abraham, I.; Joshi, R.; Pardasani, P.; Pardasani, R. T. Recent Advances in 1, 4-Benzoquinone Chemistry. *J. Braz Chem. Soc.* **2011**, *22* (3), 385−421.

(5) Dias, F.; Guerra, F.; Lima, F.; de Castro, Y.; Ferreira, V.; Campos, V.; Fernandes, P.; Cunha, A. Synthesis and Biological Evaluation of Benzo[f]Indole-4, 9-Diones N-Linked to Carbohydrate Chains as New Type of Antitumor Agents. *J. Braz Chem. Soc.* **2021**, DOI: 10.21577/0103-5053.20200202.

(6) Aminin, D.; Polonik, S. 1, 4-Naphthoquinones: Some Biological Properties and Application. *Chem. Pharm. Bull. (Tokyo)* **2020**, *68* (1), 46−57.

(7) Dulo, B.; Phan, K.; Githaiga, J.; Raes, K.; De Meester, S. Natural Quinone Dyes: A Review on Structure, Extraction Techniques, Analysis and Application Potential. *Waste Biomass Valorization* **2021**, *12* (12), 6339−6374.

(8) Leite, T. O. C.; Novais, J. S.; de Carvalho, B. L. C.; Ferreira, V. F.; Miceli, L. A.; Fraga, L.; Abrahim-Vieira, B.; Rodrigues, C. R.; Sa Figueiredo, A. M.; Castro, H. C.; Cunha, A. C. Synthesis, In Vitro and In Silico Studies of Indolequinone Derivatives against Clinically Relevant Bacterial Pathogens. *Curr. Top Med. Chem.* **2020**, *20* (3), 192−208.

(9) da Silva, W. A.; da Silva, L. C. R. P.; Campos, V. R.; de Souza, M. C. B. v; Ferreira, V. F.; dos Santos, Â. C. P. B.; Sathler, P. C.; de Almeida, G. S.; Dias, F. R. F.; Cabral, L. M.; de Azeredo, R. B. v; Cunha, A. C. Synthesis and Antitumor Evaluation of Hybrids of 5, 8-Dioxo-5, 8-Dihydroisoquinoline-4-Carboxylates ∼ and ∼ carbohydrates. *Future Med. Chem.* **2018**, *10* (5), 527−540.

(10) Campos, V. R.; Cunha, A. C.; Silva, W. A.; Ferreira, V. F.; de Sousa, C. S.; Fernandes, P. D.; Moreira, V. N.; da Rocha, D. R.; Dias, F. R. F.; Montenegro, R. C.; de Souza, M. C. B. v; da C S Boechat, F.; Franco, C. F. J.; Resende, J. A. L. C. Synthesis of a New Class of Naphthoquinone Glycoconjugates and Evaluation of Their Potential as Antitumoral Agents. *RSC Adv.* **2015**, *5* (116), 96222−96229.

(11) Varricchio, C.; Beirne, K.; Aeschlimann, P.; Heard, C.; Rozanowska, M.; Votruba, M.; Brancale, A. Discovery of Novel 2-Aniline-1,4-Naphthoquinones as Potential New Drug Treatment for Leber's Hereditary Optic Neuropathy (LHON). *J. Med. Chem.* **2020**, *63* (22), 13638.

(12) Leyva, E.; López, L. I.; de la Cruz, R. F. G.; Espinosa-González, C. G. Synthesis and Studies of the Antifungal Activity of 2-Anilino-/2,3-Dianilino-/2-Phenoxy- and 2,3-Diphenoxy-1,4-Naphthoquinones. *Res. Chem. Intermed.* **2017**, *43* (3), 1813.

(13) Becerra, N. A.; Espinosa-Bustos, C.; Vázquez, K.; Rivera, G.; Paulino, M.; Cantero, J.; Nogueda, B.; Chacón-Vargas, F.; Castillo-Velazquez, U.; Rodríguez, A. F. E.; Toledo, S.; Moreno-Rodríguez, A.; Aranda, M.; Salas, C. O. Expanding the Chemical Space of Aryloxy-Naphthoquinones as Potential Anti-Chagasic Agents: Synthesis and Trypanosomicidal Activity. *Med. Chem. Res.* **2021**, *30* (12), 2256.

(14) Chai, J.-D.; Head-Gordon, M. Long-Range Corrected Hybrid Density Functionals with Damped Atomatom Dispersion Corrections. *Phys. Chem. Chem. Phys.* **2008**, *10* (44), 6615.

(15) Hehre, W. J. Ab Initio Molecular Orbital Theory. *Acc. Chem. Res.* **1976**, *9* (11), 399−406.

(16) Hay, P. J.; Wadt, W. R. Ab Initio Effective Core Potentials for Molecular Calculations. Potentials for K to Au Including the Outermost Core Orbitals. *J. Chem. Phys.* **1985**, *82* (1), 299−310.

(17) Mennucci, B.; Cancès, E.; Tomasi, J. Evaluation of Solvent Effects in Isotropic and Anisotropic Dielectrics and in Ionic Solutions with a Unified Integral Equation Method:0.167em Theoretical Bases, Computational Implementation, and Numerical Applications. *J. Phys. Chem. B* **1997**, *101* (49), 10506−10517.
(18) Hewgill, F. R.; Mullings, L. R. Nucleophilic Substitution of Bromo-p-Benzoquinones by Dimethylamine. *Aust. J. Chem.* **1975**, *28* (11), 2561.
(19) Tandon, V. K.; Maurya, H. K. 'On Water': Unprecedented Nucleophilic Substitution and Addition Reactions with 1, 4-Quinones in Aqueous Suspension. *Tetrahedron Lett.* **2009**, *50* (43), 5896−5902.
(20) Afonin, A. V.; Ushakov, I. A.; Vashchenko, A. V.; Kondrashov, E. V.; Rulev, A. Y. GAIO, DFT, AIM and NBO Analysis of the N-H··· O Intramolecular Hydrogen-Bond Influence on the 1J (N, H) Coupling Constant in Push−Pull Diaminoenones. *Magn. Reson. Chem.* **2010**, *48* (9), 661−670.
(21) Paul, B. K.; Guchhait, N. TDDFT Investigation of the Potential Energy Surface for Excited-State Intramolecular Proton Transfer (ESIPT) Reaction of 10-Hydroxybenzo[h]Quinoline: Topological (AIM) and Population (NBO) Analysis of the Intramolecular Hydrogen Bonding Interaction. *J. Lumin.* **2011**, *131* (9), 1918−1926.
(22) Isravel, A. D.; Jeyaraj, J. K.; Thangasamy, S.; John, W. J. DFT, NBO, HOMO-LUMO, NCI, Stability, Fukui Function and Hole Electron Analyses of Tolcapone. *Comput. Theor Chem.* **2021**, *1202*, 113296.
(23) Soliman, S. M.; Hagar, M.; Ibid, F.; El Ashry, E. S. H. Experimental and Theoretical Spectroscopic Studies, HOMOLUMO, NBO Analyses and Thionethiol Tautomerism of a New Hybrid of 1, 3, 4-Oxadiazole-Thione with Quinazolin-4-One. *Spectrochim Acta A Mol. Biomol Spectrosc* **2015**, *145*, 270−279.
(24) Reed, A. E.; Weinhold, F. Natural Bond Orbital Analysis of Near-HartreeFock Water Dimer. *J. Chem. Phys.* **1983**, *78* (6), 4066−4073.
(25) Foster, J. P.; Weinhold, F. Natural Hybrid Orbitals. *J. Am. Chem. Soc.* **1980**, *102* (24), 7211−7218.
(26) Reed, A. E.; Weinstock, R. B.; Weinhold, F. Natural Population Analysis. *J. Chem. Phys.* **1985**, *83* (2), 735−746.
(27) Reed, A. E.; Curtiss, L. A.; Weinhold, F. Intermolecular Interactions from a Natural Bond Orbital, Donor-Acceptor Viewpoint. *Chem. Rev.* **1988**, *88* (6), 899−926.
(28) *The Structure of Small Molecules and Ions;*Naaman, R., Vager, Z., Eds.; Springer, 1988. DOI: 10.1007/978-1-4684-7424-4.
(29) Glendenning, E. D.; Reed, A. E.; Carpenter, J. E.; Weinhold, F.*NBO,* ver. 3.1; Gaussian Inc.: Pittsburg, PA, 2001.
(30) Frisch, M. J.; Trucks, G. W.; Schlegel, H. B.; Robb, M. A.; Barone, V.; Cheeseman, J. R.; Scalmani, G.; Mennucci, B.; Petersson, G. A.; Nakatsuji, H.; Li, X.; Hratchian, H. P.; Izmaylov, A. F.; Bloino, J.; Zheng, G.; Sonnenberg, J. L.; Hada, M.; Ehara, M.; Fukuda, R.; Hasegawa, J.; Ishida, M.; Nakajima, T.; Honda, Y.; Kitao, O.; Nakai, H.; Vreven, T.; Montgomery, J. A., Jr.; Peralta, J. E.; Ogliaro, F.; Bearpark, M.; Heyd, J. J.; Brothers, E.; Kudin, K. N.; Staroverov, V. N.; Kobayashi, R.; Normand, J.; Raghavachari, K.; Rendell, A.; Burant, J. C.; Iyengar, S. S.; Tomasi, J.; Cossi, M.; Millam, J. M.; Rega, N.; Klene, M.; Knox, J. E.; Cross, J. B.; Bakken, V.; Adamo, C.; Jaramillo, J.; Gomperts, R.; Stratmann, R. E.; Yazyev, O.; Austin, A. J.; Cammi, R.; Ochterski, J. W.; Pomelli, C.; Martin, R. L.; Morokuma, K.; Voth, G. A.; Zakrzewski, V. G.; Salvador, P.; Dannenberg, J. J.; Daniels, A. D.; Dapprich, S.; Farkas, Ö.; Foresman, J. B.; Ortiz, V.; Cioslowski, J.; Fox, D. J.*Gaussian 09,* rev. D.01; Gaussian, Inc., 2009.
(31) Mulliken, R. S. Electronic Population Analysis on LCAOMO Molecular Wave Functions. I. *J. Chem. Phys.* **1955**, *23* (10), 1833−1840.
(32) Breneman, C. M.; Wiberg, K. B. Determining Atom-Centered Monopoles from Molecular Electrostatic Potentials. The Need for High Sampling Density in Formamide Conformational Analysis. *J. Comput. Chem.* **1990**, *11* (3), 361−373.
(33) Hirshfeld, F. L. Bonded-Atom Fragments for Describing Molecular Charge Densities. *Theor Chim Acta* **1977**, *44* (2), 129−138.
(34) Ritchie, J. P.; Bachrach, S. M. Some Methods and Applications of Electron Density Distribution Analysis. *J. Comput. Chem.* **1987**, *8* (4), 499−509.
(35) Francl, M. M.; Chirlian, L. E. The Pluses and Minuses of Mapping Atomic Charges to Electrostatic Potentials. *Rev. Comput. Chem.* **2007**, *14*, 1−31.
(36) Marenich, A. v; Jerome, S. v; Cramer, C. J.; Truhlar, D. G. Charge Model 5: An Extension of Hirshfeld Population Analysis for the Accurate Description of Molecular Interactions in Gaseous and Condensed Phases. *J. Chem. Theory Comput* **2012**, *8* (2), 527−541.
(37) Reed, A. E.; Weinstock, R. B.; Weinhold, F. Natural Population Analysis. *J. Chem. Phys.* **1985**, *83* (2), 735−746.
(38) Otero-de-la-Roza, A.; Johnson, E. R.; Contreras-García, J. Revealing Non-Covalent Interactions in Solids: NCI Plots Revisited. *Phys. Chem. Chem. Phys.* **2012**, *14* (35), 12165.
(39) Lu, T.; Chen, F. Multiwfn: A Multifunctional Wavefunction Analyzer. *J. Comput. Chem.* **2012**, *33* (5), 580−592.
(40) Fonseca Guerra, C.; Handgraaf, J.-W.; Baerends, E. J.; Bickelhaupt, F. M. Voronoi Deformation Density (VDD) Charges: Assessment of the Mulliken, Bader, Hirshfeld, Weinhold, and VDD Methods for Charge Analysis. *J. Comput. Chem.* **2004**, *25* (2), 189−210.
(41) Wiberg, K. B.; Rablen, P. R. Atomic Charges. *J. Org. Chem.* **2018**, *83* (24), 15463−15469.
(42) Wang, B.; Li, S. L.; Truhlar, D. G. Modeling the Partial Atomic Charges in Inorganometallic Molecules and Solids and Charge Redistribution in Lithium-Ion Cathodes. *J. Chem. Theory Comput* **2014**, *10* (12), 5640−5650.
(43) Kenouche, S.; Belkadi, A.; Djebaili, R.; Melkemi, N. High Regioselectivity in the Amination Reaction of Isoquinolinequinone Derivatives Using Conceptual DFT and NCI Analysis. *J. Mol. Graph Model* **2021**, *104*, 107828.
(44) Chattaraj, P. K.; Lee, H.; Parr, R. G. HSAB Principle. *J. Am. Chem. Soc.* **1991**, *113* (5), 1855−1856.
(45) Pearson, R. G.The HSAB Principle. In *Chemical Hardness;*Wiley-VCH Verlag GmbH & Co. KGaA, 2005; pp 1−27. DOI: 10.1002/3527606173.ch1.
(46) Nguyen, L. T.; Le, T. N.; De Proft, F.; Chandra, A. K.; Langenaeker, W.; Nguyen, M. T.; Geerlings, P. Mechanism of [2 1] Cycloadditions of Hydrogen Isocyanide to Alkynes:0.167em Molecular Orbital and Density Functional Theory Study. *J. Am. Chem. Soc.* **1999**, *121* (25), 5992−6001.
(47) Saha, S.; Bhattacharjee, R.; Roy, R. K. Hardness Potential Derivatives and Their Relation to Fukui Indices. *J. Comput. Chem.* **2013**, *34* (8), 662−672.
(48) Franco-Pérez, M.; Polanco-Ramírez, C. A.; Gázquez, J. L.; Ayers, P. W.Local and Nonlocal Counterparts of Global Descriptors: The Cases of Chemical Softness and Hardness. *J. Mol. Model.***2018**, *24* (10). DOI: 10.1007/s00894-018-3823-4.
(49) Uzun, S.; Esen, Z.; Koç, E.; Usta, N. C.; Ceylan, M. Experimental and Density Functional Theory (MEP, FMO, NLO, Fukui Functions) and Antibacterial Activity Studies on 2-Amino-4-(4-Nitrophenyl) −5, 6-Dihydrobenzo [h] Quinoline-3-Carbonitrile. *J. Mol. Struct.* **2019**, *1178*, 450−457.
(50) Sebastian, S. H. R.; Al-Alshaikh, M. A.; El-Emam, A. A.; Panicker, C. Y.; Zitko, J.; Dolezal, M.; VanAlsenoy, C. Spectroscopic, Quantum Chemical Studies, Fukui Functions, In vitro Antiviral Activity and Molecular Docking of 5-Chloro-N-(3-Nitrophenyl)-Pyrazine-2-Carboxamide. *J. Mol. Struct.* **2016**, *1119*, 188−199.
(51) Koopmans, T. Über Die Zuordnung von Wellenfunktionen Und Eigenwerten Zu Den Einzelnen Elektronen Eines Atoms. *physica* **1934**, *1* (1−6), 104−113.
(52) Parr, R. G.; Yang, W. Density Functional Approach to the Frontier-Electron Theory of Chemical Reactivity. *J. Am. Chem. Soc.* **1984**, *106* (14), 4049−4050.
(53) Parr, R. G. Density Functional Theory of Atoms and Molecules. *Horizons of Quantum Chemistry* **1980**, 5−15.
(54) Olah, J.; Van Alsenoy, C.; Sannigrahi, A. B. Condensed Fukui Functions Derived from Stockholder Charges: Assessment of Their

https://doi.org/10.1021/acsomega.2c04607
ACS Omega 2022, 7, 40241−40256

Performance as Local Reactivity Descriptors. *J. Phys. Chem. A* **2002**, *106* (15), 3885.
(55) Gilardoni, F.; Weber, J.; Chermette, H.; Ward, T. R. Reactivity Indices in Density Functional Theory: A New Evaluation of the Condensed Fukui Function by Numerical Integration. *J. Phys. Chem. A* **1998**, *102* (20), 3607.
(56) de Luca, G.; Sicilia, E.; Russo, N.; Mineva, T. On the Hardness Evaluation in Solvent for Neutral and Charged Systems. *J. Am. Chem. Soc.* **2002**, *124* (7), 1494.
(57) Mineva, T.; Sicilia, E.; Russo, N. Density-Functional Approach to Hardness Evaluation and Its Use in the Study of the Maximum Hardness Principle. *J. Am. Chem. Soc.* **1998**, *120* (35), 9053.
(58) Mineva, T.; Parvanov, V.; Petrov, I.; Neshev, N.; Russo, N. Fukui Indices from Perturbed Kohn-Sham Orbitals and Regional Softness from Mayer Atomic Valences. *J. Phys. Chem. A* **2001**, *105* (10), 1959.
(59) Mineva, T.; Russo, N. Atomic Fukui Indices and Orbital Hardnesses of Adenine, Thymine, Uracil, Guanine and Cytosine from Density Functional Computations. *J. Mol. Struct.* **2010**, *943* (1−3), 71.
(60) Yang, W.; Mortier, W. J. The Use of Global and Local Molecular Parameters for the Analysis of the Gas-Phase Basicity of Amines. *J. Am. Chem. Soc.* **1986**, *108* (19), 5708−5711.
(61) Demircioğlu, Z.; Kaştaş, Ç. A.; Büyükgüngör, O. Theoretical Analysis (NBO, NPA, Mulliken Population Method) and Molecular Orbital Studies (Hardness, Chemical Potential, Electrophilicity and Fukui Function Analysis) of (*E*)-2-((4-Hydroxy-2-Methylphenylimino)Methyl)-3-Methoxyphenol. *J. Mol. Struct.* **2015**, *1091*, 183.
(62) Thanikaivelan, P.; Padmanabhan, J.; Subramanian, V.; Ramasami, T. Chemical Reactivity and Selectivity Using Fukui Functions: Basis Set and Population Scheme Dependence in the Framework of B3LYP Theory. *Theor Chem. Acc. 2002 107:6* **2002**, *107* (6), 326−335.
(63) Caldwell, S. T.; McPhail, D. B.; Duthie, G. G.; Hartley, R. C. Synthesis of Polyhydroxylated Flavonoids Bearing a Lipophilic Decyl Tail as Potential Therapeutic Antioxidants. *Can. J. Chem.* **2012**, *90* (1), 23−33.
(64) Deya, P. M.; Dopico, M.; Morey, A. G. R. J.; Saa, J. M. On the Regioselectivity of the Fremys Salt Oxidation of Phenols. *Tetrahedron* **1987**, *43* (15), 3523−3532.
(65) Cao, C.-T.; Chen, M.; Fang, Z.; Au, C.; Cao, C. Relationship Investigation between C(Sp2)X and C(Sp3)X Bond Energies Based on Substituted Benzene and Methane. *ACS Omega* **2020**, *5* (30), 19304−19311.
(66) Li, X.-H.; Li, T.-W.; Ju, W.-W.; Yong, Y.-L.; Zhang, X.-Z. Molecular Structure, Vibrational Spectra, NBO Analysis and Molecular Packing Prediction of 3-Nitroacetanilide by Ab Initio HF and Density Functional Theory. *Spectrochim Acta A Mol. Biomol Spectrosc* **2014**, *118*, 503−509.
(67) Yadav, J. S.; Reddy, B. V. S.; Swamy, T.; Shankar, K. S. Green Protocol for Conjugate Addition of Amines to P-Quinones Accelerated by Water. *Monatsh. Chem.* **2008**, *139* (11), 1317.
(68) Bruker. *APEX2* and SAINT; Bruker AXS Inc.: Madison, WI, 2007.
(69) *SAINT,* B. V8. 34A; Bruker AXS: Madison, WI, 2013.
(70) Sheldrick, G. M.SADABS, Program for Empirical Absorption Correction of Area Detector Data. In *SADABS;*University of Gottingen, 1996.
(71) Sheldrick, G. M. Crystal Structure Refinement WithSHELXL. *Acta Crystallogr. C Struct Chem.* **2015**, *71* (1), 3−8.
(72) Sheldrick, G. M. SHELXT Integrated Space-Group and Crystal-Structure Determination. *Acta Crystallogr. A Found Adv.* **2015**, *71* (1), 3−8.
(73) Dolomanov, O. v; Bourhis, L. J.; Gildea, R. J.; Howard, J. A. K.; Puschmann, H. OLEX2: A Complete Structure Solution, Refinement and Analysis Program. *J. Appl. Crystallogr.* **2009**, *42* (2), 339−341.

https://doi.org/10.1021/acsomega.2c04607
ACS Omega 2022, 7, 40241−40256